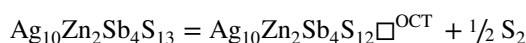**ORIGINAL PAPER**

Sulfur vacancies in fahlores from the Ag-Pb–Zn Mangazeyskoye ore deposit (Sakha, Russia)

Richard O. Sack[1] · Natalia G. Lyubimtseva[2] · Nikolay S. Bortnikov[2] · Elena Yu Anikina[2] · Sergey E. Borisovsky[2]
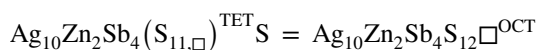
Abstract

Fahlores from the epithermal Mangazeyskoye Ag-Pb–Zn ore deposit (Sakha, Russia) typically occur in rhythmically zoned crystals. In contrast to typical $(Ag,Cu)_{10}(Fe,Zn)_2Sb_4S_{13}$ fahlores, up to about 2.6 of the 13 sulfur atoms in the formula unit may be vacant and many of them have $Ag/(Ag+Cu)$ ratios substantially above those established for $(Ag,Cu)_{10}(Fe,Zn)_2Sb_4S_{13}$ fahlores coexisting with miargyrite, pyrargyrite, and sphalerite by experimental, field, and theoretical investigations. The charge balance inequalities consequent on the removal of sulfur are compensated by metallization of the nominally Ag^+ and Cu^+ ions in the octahedral metal clusters that are formed by the removal of S^{2-} from the octahedral site at the center and corners of the unit cell of fahlore (space group $I\bar{4}3m$, Z = 2). The development of these vacancies leads to an effective ionic charge of $[(Ag, Cu)_6^{(6-2*vac)+}]$ for these octahedral clusters, resulting in an intrinsic limit on sulfur vacancies of 3 per formula unit (pfu). The increases in the $Ag/(Ag+Cu)$ ratio of some of the Mangazeyskoye fahlores relative to those defined for $(Ag,Cu)_{10}(Fe,Zn)_2Sb_4S_{13}$ fahlores are readily attributed to the lowering of the activities of $Ag_{10}Zn_2Sb_4S_{13}$ and $Ag_{10}Fe_2Sb_4S_{13}$ components in fahlore by sulfur vacancies. This results in expansion of the field of fahlore stability relative to that given by the fahlore breakdown reaction $Ag_{10}Zn_2Sb_4S_{13}$ (fahlore) $= AgSbS_2$ (miargyrite) $+ 3\ Ag_3SbS_3$ (pyrargyrite) $+ 2$ ZnS (sphalerite) for $(Ag,Cu)_{10}(Fe,Zn)_2Sb_4S_{13}$ fahlores. A preliminary analysis demonstrates that the increased $Ag/(Ag+Cu)$ ratios observed in the Mangazeyskoye fahlores relative to those defined for $(Ag,Cu)_{10}(Fe,Zn)_2Sb_4S_{13}$ fahlores are due to sulfur vacancies being almost exclusively in the octahedral sulfur site where the vacancy for sulfur substitution appears to be approximately ideal. However, it appears that a maximum in $Ag/(Ag+Cu)$ ratios is reached around one pfu, and, to a first approximation, does not appear to increase with further increase in contents. This latter inference suggests that the for S ($\square(S)_{-1}$) substitution on tetrahedral sulfur sites may be highly nonideal. When properly calibrated for sulfur fugacity based on experimental, spectroscopic, and theoretical studies, reactions such as

$$Ag_{10}Zn_2Sb_4S_{13} = Ag_{10}Zn_2Sb_4S_{12}\square^{OCT} + \tfrac{1}{2}\ S_2$$

and

$$Ag_{10}Zn_2Sb_4(S_{11,\square})^{TET}S = Ag_{10}Zn_2Sb_4S_{12}\square^{OCT}$$

will afford fahlore to serve as a petrogenetic indicator of sulfur fugacity in low-sulfidation environments. Until such calibrations are developed, the fahlore $Ag/(Ag+Cu)$ ratios may nonetheless be used to define relative sulfur fugacities in rhythmically zoned fahlores from ore deposits such as Mangazeyskoye.

Communicated by Timothy L. Grove.

✉ Richard O. Sack
  fahlore@gmail.com

1   OFM Research Corporation, Redmond, WA 98053, USA

2   Institute of Geology of Ore Deposits, Petrography, Mineralogy and Geochemistry of the Russian Academy of Sciences, 35 Staromonetny pereulok, Moscow 119017, Russia

Introduction

Fahlore (tetrahedrite group minerals)[1] is a natural solid
solution that is the most common economic ore mineral of
silver in Ag–Pb–Zn and bonanza Ag-Au deposits (Sack and
Loucks 1985). It has recently been found that fahlore can
exhibit high-thermoelectric performance and serve as highly
efficient thermoelectric materials for waste heat recovery
applications (e.g., Fan et al. 2013). These features of fahlore
cause unrelenting interest in it among researchers. Its crystal
chemical composition typically approximates the simple stoi-
chiometry $\sim {}^{III}(Ag^+, Cu^+)_6 {}^{IV}((Cu^+, Ag^+)_{2/3}(Zn^{2+}, Fe^{2+})_{1/3})_6$
${}^{III}(Sb^{3+}, As^{3+})_4 {}^{IV}(S^{2-}, Se^{2-})_{12} {}^{VI}(S^{2-}, Se^{2-}, \square)$ (space group $I\bar{4}3m$, Z=2), the sulfur vacancy-free varieties correspond-
ing to an ideal crystal structure with 208 valance electrons
per unit cell and full occupancy of the 6 trigonal-planar
(TRG), 6 tetrahedral (TET), and 4 semimetal (SM) sites in
the l3-sulfur formula unit (e.g., Pauling and Neuman 1934;
Wuensch 1964; Johnson and Jeanloz 1983; Biagioni et al.
2020). Pauling and Neuman (1934) reappraised Machatsch-
ki's (1928) solution of the crystal structure, interpreting it
as a "complex defect derivative" of the sphalerite structure.
Wuensch (1964) and Wuensch et al. (1966) clearly indicate
that Pauling and Neuman's interpretation, still prevalent in
current mineralogical literature, is at best misleading. The
concept that the fahlore crystal structure is a framework
analogous to sodalite has been suggested (Belov and Pobe-
dimskaya 1973; Johnson et al. 1988). Synthetic fahlores in
the Cu-Sb-S, Cu-As-S, Fe-Cu-Sb-S and Fe-Cu-As-S systems
show considerable variation in the number of atoms per for-
mula unit (that is, the number of atoms per 13 sulfurs). For
example, the compositional field in the Cu-Sb-S system lies
within the range $Cu_{12}Sb_4S_{13} - Cu_{14}Sb_4S_{13} - Cu_{12}Sb_{4.67}S_{13}$
(Tatsuka and Morimoto 1977; Makovicky and Skinner
1978). Although the chemical compositions of synthetic
analogues of fahlores typically deviate from the simple
stoichiometric formula, their crystal structures have been
considered to have the same space group symmetry, $I\bar{4}3m$.
The results of electron microprobe analysis of natural fahlore
are not always satisfactorily converted to a simple stoichio-
metric formula (Lyubimtseva et al. 2018). Thus, there is a
paradox when the data on the chemical composition and

crystal structure of the mineral do not agree. This effect is
especially enhanced if we turn to silver-containing fahlores.

Several recent studies of the stoichiometry and
cell dimensions of Ag-rich compositions of the com-
plex sphalerite derivative structure fahlore have recog-
nized new approved endmembers and assigned them
new names (e.g., $Ag_{10}(Zn,Fe)_2Sb_4S_{13}$, "rozhdestvens-
kayaite"; $Ag_6Cu_4(Fe,Zn)_2Sb_4S_{13}$, "argentotetrahedrite";
$Ag_6Ag_4(Fe,Zn)_2-As_4S_{13}$, "zvêstovite"; Welch et al. 2018;
Sejkora et al. 2021a) and have also recognized their addi-
tional hypothetical Fe, Zn, and Hg endmembers (Biagioni
et al. 2020; Sejkora et al. 2021b, 2022; Wu et al. 2021), and
Zn and Fe endmembers components of "kenoargentotetra-
hedrite", in which the sulfur in octahedral coordination by
Cu and Ag at the corners and center of the unit cell is vacant
or absent, $Ag_6Cu_4(Fe,Zn)_2Sb_4S_{12}$, (e.g., Moëlo et al. 2008;
Biagioni et al. 2020; Qu et al. 2021). These studies conclude
that the cell edges of Sb-fahlores with 13 sulfur atoms in
their formula increase linearly between Cu and Ag endmem-
bers and that the decrease in cell edges that is observed in
some natural fahlores with Ag/(Ag+Cu) greater than about
0.4 is due to substitution of vacancies for sulfur in the octa-
hedrally coordinated site (e.g., Riley 1974; Balitskaya et al.
1989; Rozhdestvenskaya et al. 1993). However, Ebel (1993)
synthesized a $(Ag_{0.73},Cu_{0.27})_{10}Zn_2Sb_4S_{13}$ fahlore at 400 °C
with a cell edge dimension of 10.7867 ± 0.004 angstroms on
quenching, consistent with the linear trend of increasing cell
edge with Ag/(Ag+Cu) ratio established in the synthesis
experiments of Pattrick and Hall (1983) and that of rozhdest-
venskayaite (Welch et al. 2018, their Fig. 2), but this fahlore
exhibited a contraction in its cell edge to 10.6283 ± 0.007
angstroms when annealed at 150 °C for 891 h (cf., Sack and
Ebel 2006, Fig. 43). We had initially assumed that the cell
edge of Ebel's fahlore might come to closely approach the
trends of the collapsing cell edges of Riley (1974), Balits-
kaya et al. (1989) and Rozhdestvenskaya et al. (1993), but
then realized that a close approach of their cell edges was
improbable on the traditional cell edge versus Ag or Ag/
(Ag+Cu) diagram, because we would be comparing a sulfur
vacancy-free fahlore with sulfur vacancy-bearing fahlores
(e.g., the average sulfur vacancy content of the 12 fahlores
examined by Balitskaya et al. (1989) is 0.572 ± 0.344 pfu
when the formulae of their fahlores are calculated on a 16
metal+semi-metal basis). Clearly the traditional two-dimen-
sional representation of cell edge versus Ag or Ag/(Ag+Cu)
diagram is a canard, as, at a minimum, the cell edge lengths
of Sb fahlores are a function of Ag or Ag/(Ag+Cu) and
sulfur vacancy contents at a given temperature, and there-
fore a three-dimensional representation of these quantities
should be contoured for annealing temperature (i.e., a four-
dimensional representation is required).

---

[1] "Tetrahedrite group minerals" is a new name of the fahlore group
approved by the Commission on New Minerals of the International
Mineralogical Association (Biagioni et al., 2020). In our work we
will use the historical term "fahlore" to preserve the continuity of
generations.

In addition, the thermodynamic quantity for Fe-Zn exchange between $(Cu,Ag)_{10}(Fe,Zn)_2Sb_4S_{13}$ fahlores and $(Zn,Fe)S$ sphalerites, $RT\ln[(X_{Fe}^{Fah}/X_{Zn}^{Fah}) \cdot (a_{ZnS}^{Sph}/a_{FeS}^{Sph})]$ (where a is activity), is not a linear function of $Ag/(Ag+Cu)$ in fahlore at a given $X_{ZnS}^{Sph}/X_{FeS}^{Sph}$ ratio and temperature (O'Leary and Sack 1987) as this quantity is for $Cu_{10}(Fe,Zn)_2(As,Sb)_4S_{13}$ fahlores with $As/(As+Sb)$ ratio (Sack and Loucks 1985; O'Leary and Sack 1987). Instead, this quantity has a sigmoid shape with respect to $Ag/(Ag+Cu)$ in fahlore at a given temperature and FeS/ZnS ratio in $(Zn,Fe)S$ sphalerite. It displays both a local maximum and minimum with increasing $Ag/(Ag+Cu)$ ratio. Furthermore, the maxima and minima for varying temperatures and FeS/ZnS ratios in $(Zn,Fe)S$ sphalerite lie respectively above and below the lines defined by the $Ag_{10}(Fe,Zn)_2Sb_4S_{13}$ and $Cu_{10}(Fe,Zn)_2Sb_4S_{13}$ endmembers.

To describe these relations O'Leary and Sack (1987) formulated a simple thermodynamic model which makes explicit provision for Ag–Cu ordering between trigonal-planar and tetrahedral sites in $(Cu,Ag)_{10}(Fe,Zn)_2Sb_4S_{13}$ fahlores. They discovered that all calibrations of this model that complied with their constraints on this Zn-Fe exchange reaction required that Ag changes its preference for trigonal-planar to tetrahedral sites with increasing $Ag/(Ag+Cu)$ ratio. They also discovered that all viable calibrations of this model required that there are low-temperature ($T < 200$ °C) miscibility gaps in $(Cu,Ag)_{10}(Fe,Zn)_2Sb_4S_{13}$ fahlores. This latter prediction was subsequently confirmed by the discovery of such miscibility gaps in fahlores from multiple ore deposits (e.g., Sack et al. 2003, Fig. 1 here; Chinchilla et al. 2016, Fig. 16; Zhai et al. 2019, Fig. 11 and Fig. 1 here; Alves et al. 2022, Fig. 8b; Zhai 2022, Figs. 4b, 5).

In addition to satisfy the scientific method, the inferences about the structural role of Ag in $(Cu,Ag)_{10}(Fe,Zn)_2Sb_4S_{13}$ fahlores of O'Leary and Sack (1987) are consistent with the principles of thermodynamics and statistical mechanics, as they predict that Ag and Cu will become increasingly disordered between trigonal-planar and tetrahedral sites with increasing temperature, and thus will trend toward linear volume—composition relations with increasing temperature. This sharply contrasts with the "universally" agreed upon assumption of the sulfide mineralogical community who pronounce, for example, that "substitution by Ag, is universally assumed to start in the triangular sites and spill over into tetrahedral sites only when the former are (nearly) filled" (Makovicky 2006, p. 54). Clearly, the results of Ebel (1993) demonstrate that the linear trend of cell edge lengths established by the synthesis experiments of Pattrick and Hall (1983) and Ebel (1993), and that of $Ag_{10}Zn_2Sb_4S_{13}$ (rozhdestvenskayaite) determined by Welch et al. (2018), may only be appropriate for temperatures of about 400 °C,

because the results of the annealing experiment of Ebel (1993) demonstrates that the cell-edge lengths, and hence the ordering of Ag and Cu between trigonal—planer (i.e., triangular) and tetrahedral sites, are strongly temperature dependent, as required by thermodynamics and statistical mechanics. The thermodynamically challenged interpretation that cell edge lengths of $(Ag,Cu)_{10}Zn_2Sb_4S_{13}$ are linear in $Ag/(Ag+Cu)$ ratios is also perpetuated by Biagioni et al. (2020, their Fig. 2) who depict data of the Shimada and Hirowatari (1972) for natural $(Ag,Cu)_{10}(Fe,Zn)_2Sb_4S_{13}$ fahlores as if their cell edge lengths are consistent with a roughly linear relationship between Cu and Ag endmembers, despite the fact that Shimada and Hirowatari (1972) only determined cell edge lengths for fahlores with $Ag/(Ag+Cu)$ ratios < 0.4.

The generally accepted assumption that Ag strongly prefers the trigonal-planar site independent of $Ag/(Ag+Cu)$ ratio is also inconsistent with the observed compositions of the binodes of the low-temperature (i.e., $T < 200$ °C) miscibility gaps in $(Cu,Ag)_{10}(Fe,Zn)_2Sb_4S_{13}$ fahlores (e.g., Sack et al. 2003, their Table 1; Fig. 1 here). Because Makovicky (2006) and others (e.g., Moëlo et al. 2008; Welch et al. 2018; Biagioni et al. 2020) allege that Ag enters only the trigonal-planar sites until they are completely (or very nearly) full, miscibility gaps between Cu- and Ag-rich fahlores with less than 6 Ag apfu would not achieve the binode compositions observed in nature, unless asymmetric solution parameters describing the nonideality of mixing of Ag and Cu on trigonal—planar sites were of such different magnitude as to be grossly physically implausible (cf. Sack 2021, Fig. 1 and associated discussion).

Finally, a spectacular example in the list of physically implausible interpretations by mineralogical "spectroscopists" is provided by the study of Pring et al. (2008). They conclude that Fe and Zn display a disordered distribution on the metal sublattice of sphalerite based on their analyses of the infrared spectra of a series of natural sphalerites with differing Fe/Zn ratios. In reaching their conclusion they ignored the wealth of experimental data constraining $(Zn,Fe)S$ sphalerite equilibria (cf. subsequent discussion) and literature in solid-state physics (e.g., Furdyna 1988; Twardowksi et al. 1988; Twardowksi 1990) that clearly demonstrate otherwise (e.g., Toulmin et al. 1991). Fortunately, Wright and Gale (2010) performed Ab initio quantum mechanical calculations that demonstrated that Fe–Fe pair formation is favored in dilute Fe sphalerites, there are no energetic barriers to pair or larger cluster formation in more Fe-rich sphalerites (e.g., Balabin and Sack 2000; Osadchii and Gorgbaty 2010) and inferred that infrared spectroscopy may not be able to differentiate between different configurations of Fe and Zn on the metallic sublattice. Unfortunately these definitive findings from
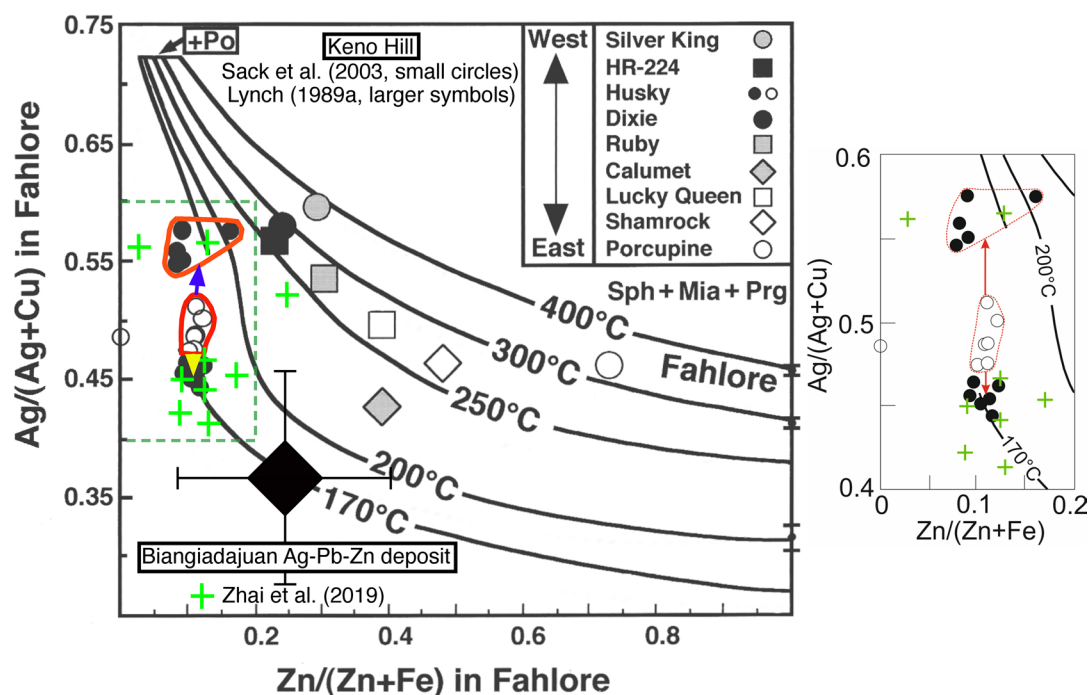
Fig. 1 Isotherms for the molar Ag/(Ag+Cu) and Zn/(Zn+Fe) ratios of $(Cu,Ag)_{10}(Fe,Zn)_2Sb_4S_{13}$ fahlores in the miargyrite + pyrargyrite + sphalerite assemblage calculated by Sack (2005, solid curves) compared with fahlore data of Lynch (1989a) and Sack et al. (2003) from mines in the Keno Hill mining district indicated in the legend in the upper right corner, and the data for primary fahlores from the Biangiadajuan Ag-Pb-Zn deposit (Inner Mongolia, China) reported by Zhai et al. (2019). The larger symbols in the legend in the upper right corner represent the average Ag/(Ag+Cu) and Zn/(Zn+Fe) ratios for high-Ag fahlores from mines in the Keno Hill Ag-Pb-Zn district reported by Lynch (1989a). Six out of eight of these average compositions have molar Ag/(Ag+Cu) and Zn/(Zn+Fe) ratios which yield temperatures from the calibration of Sack (2005, solid curves) between the 250 and 310 °C established for the main stage of mineralization from fluid inclusions in quartz and siderite by Lynch (1989b). Average Ag/(Ag+Cu) and Zn/(Zn+Fe) ratios of fahlores from the Homestake, Onek, Sadie and Husky mines reported by Lynch (1989a) are not displayed individually, because the ores containing them exhibit significant evidence of retrograde re-equilibration as reflected by significant concentrations of epithermal minerals and have fahlores with a collective average of Ag/(Ag+Cu) and Zn/(Zn+Fe) ratios, 0.367 ± 0.090 and 0.244 ± 0.159, in accord with a temperature of about 170 °C, as deduced from the calibration displayed in this figure. The large black diamond represents this collective average and the lines emanating from it indicate its associated 1σ error bars. Smaller symbols represent Ag/(Ag+Cu) and Zn/(Zn+Fe) ratios from portions of a grain of fahlore from the Husky mine which appears to have undergone unmixing reported by Sack et al. (2003), a grain in which homogeneous regions (open circles) are intermixed with regions which appear to be the result of unmixing of these homogeneous regions into Ag-rich and Ag-poor compositions (filled circles). This composite grain is in an assemblage containing stephanite (T < 197 °C, Keighin and Honea 1969); microprobe analyses from the homogeneous regions of the grain (open circles) and Ag-rich unmixed portions of the grain are enclosed by red polygons and blue and yellow arrows indicate the sense of unmixing of homogeneous portions of the grain into relatively Ag-rich and Ag-poor compositions (both represented by filled black circles). These points are further clarified by an expansion of the composition field for fahlores with Ag/(Ag+Cu) and Zn/(Zn+Fe) ratios between 0.4 and 0.6 and between 0.0 and 0.2, respectively, that appears to the right of the main figure. It is noteworthy that the Ag-rich and Ag-poor compositions agree with the calculated miscibility gaps of Sack (2005) for a temperature of about 170 °C, a temperature in accord with the presence of stephanite in the Husky Mine assemblage. The inflections in the 200 °C and 170 °C isotherms calculated by Sack (2005) reflect the close approach to the critical temperature of fahlore and the emergence of the subcritical two fahlore miscibility gap, respectively. Green crosses represent Ag/(Ag+Cu) and Zn/(Zn+Fe) ratios and 1σ uncertainties of primary fahlores from the Biangiadajuan Ag-Pb–Zn deposit (Inner Mongolia, China) reported by Zhai et al. (2019). Previous fluid inclusion studies (Wang 2014; Ruan et al. 2015) indicate that the temperatures for Ag-dominant sulfosalt formation where between ~ 160 – 250 °C and < 150 °C for final calcite formation. These temperatures are in accord with those inferred from the Ag/(Ag+Cu) – Zn/(Zn+Fe) isotherms for $(Cu,Ag)_{10}(Fe,Zn)_2Sb_4S_{13}$ fahlores by Sack (2005). The Ag/(Ag+Cu) – Zn/(Zn+Fe) ratios of the Biangiadajuan fahlores are also consistent with the miscibility gap relations inferred by Sack (2005, 2017) for these temperatures. Dots and 1σ error bars on the vertical axis for Zn/(Zn+Fe) = 1.00 represent means and standard deviations of molar Ag/(Ag+Cu) ratios of $(Cu,Ag)_{10}Zn_2Sb_4S_{13}$ fahlores at 200, 300, and 400 °C determined in the experiments of Ebel and Sack (1994). Modified from Sack (2005)

first-principle, quantum mechanical calculations have not prevented the continued appearance of models for the thermodynamic properties of (Zn,Fe)S sphalerites based on the assumption of random mixing of Fe and Zn on the metallic sublattice, models which require large excess entropies of mixing to attempt to conform to the experimental
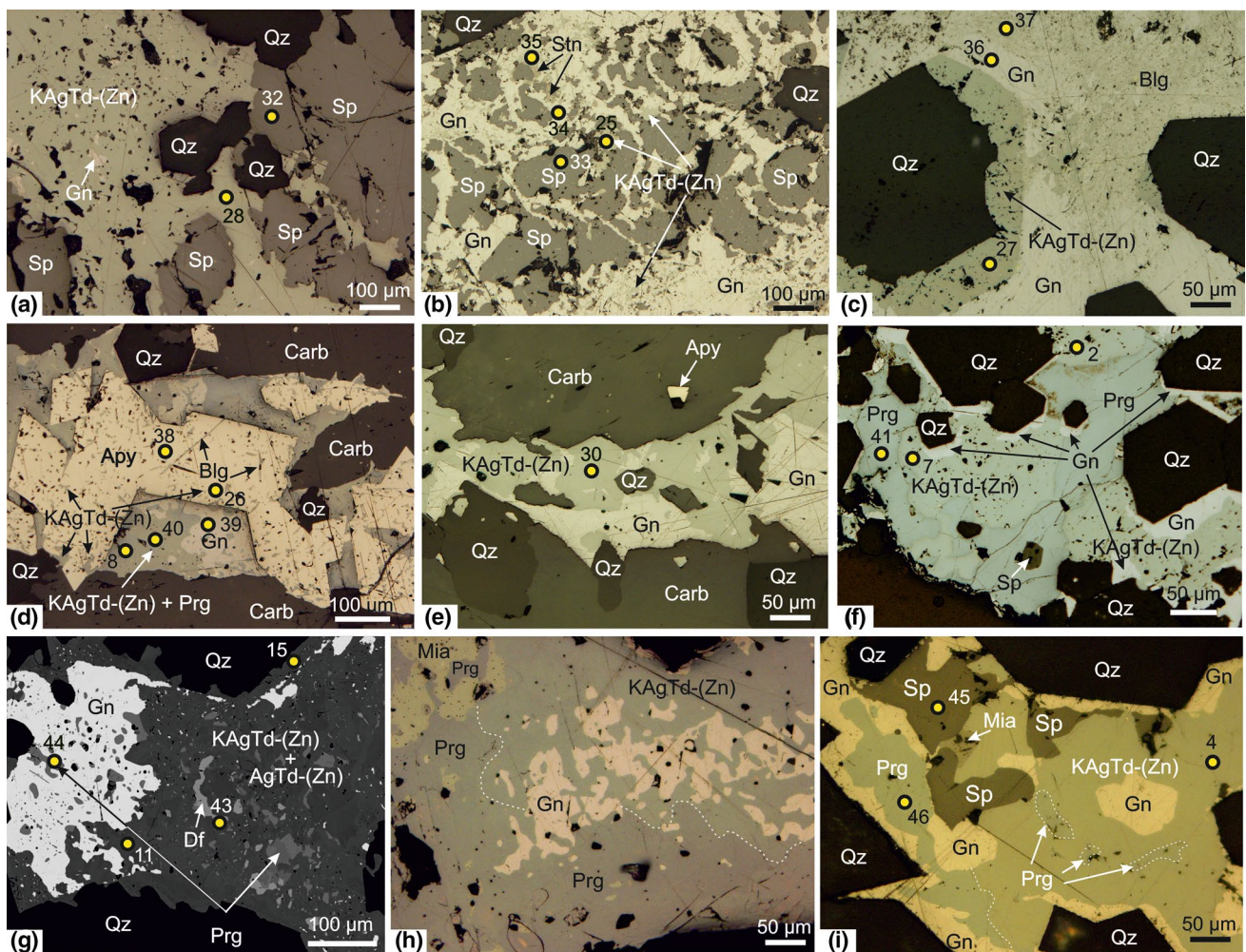
Fig. 2 Reflective light (**a–f**, **h**, **i**) and BSE (**g**) images of intergrowths of fahlore with sulfides, sulfosalts, carbonate and quartz at the Mangazeyskoye deposit: (**a**) Intergrowths of kenoargentotetrahedrite-(Zn) (KAgTd), sphalerite (Sp), galena (Gn) and quartz (Qz and other black). **b** Intergrowths of kenoargentotetrahedrite-(Zn), sphalerite, galena and stannite (Stn). The stannite-kenoargentotetrahedrite-galena aggregate replaces sphalerite with varying degrees of intensity. In the right part of the photo, the primary collomorphic-zonal texture of sphalerite grains is partially preserved: late minerals form concentrically similar areas between sphalerite relics. **c** Intergrowths of kenoargentotetrahedrite-(Zn), galena and boulangerite (Blg). Kenoargentotetrahedrite-(Zn) pseudomorphically replaces quartz along the periphery, preserving the original outlines of well-formed faces of quartz crystals. Galena and boulangerite display intimate and thin intergrowths. **d** Intergrowths of kenoargentotetrahedrite-(Zn), galena, pyrargyrite (Prg) and arsenopyrite (Apy) filling interstices between quartz and carbonate (Carb) grains. Arsenopyrite contains boulangerite needle inclusions and xenomorphic aggregates of kenoargentotetrahedrite-(Zn). **e** Intergrowths of kenoargentotetra-

hedrite-(Zn) and galena in interstices between of quartz and carbonate grains. The kenoargentotetrahedrite-galena aggregate contains xenomorphic quartz inclusions with corroded (dissolved) boundaries. **f** Intergrowths of kenoargentotetrahedrite-(Zn), galena and pyrargyrite in interstices between quartz grains. Galena forms rims around quartz crystals. Quartz retains its primary euhedral form of crystals at contact with galena and pyrargyrite. Kenoargentotetrahedrite-(Zn) corrodes quartz grains. **g** Fine intergrowth of kenoargentotetrahedrite-(Zn) and galena containing single mineral inclusions of quartz, pyrargyrite and diaphorite (Df) or their intergrowths; sometimes small inclusions of miargyrite occur in such intergrowths. **h** Intergrowths of kenoargentotetrahedrite-(Zn), galena, pyrargyrite and miargyrite (Mia). **i** Intergrowths of kenoargentotetrahedrite-(Zn), galena, pyrargyrite, miargyrite and sphalerite in interstices between quartz crystals. White arrows show intergrowths of pyrargyrite in kenoargentotetrahedrite-(Zn) highlighted in areas enclosed with white dotted lines. Circles and associated numbers indicate the location of analyses given in Table 1. Images are from Mg-1 (**d**, **e**, **g–i**), Mg-2 (**a**), Mg-3 (**f**, **h**), Mg-4 (**c**), and Mg-8 (**b**) samples.

phase equilibrium data. These large excess entropies of mixing are in gross violation of the results of the calorimetric study of Pankratz and King (1965), a study which

demonstrates conclusively that any excess entropy of mixing is negligible. This state of affairs prompts us to repeat a quote attributed to the late, distinguished metallurgical

Table 1 Representative microprobe analyses of fahlore, sulfides, and sulfosalts from the Mangazeyskoe deposit

Fahlore

Coexisting with Ag-sulfosalts (pyrargyrite, miargyrite, diaphorite, stephanite)

An. no	Sample	Mineral	unit	Ag	Cu	Zn	Fe	Pb	Sn	Sb	As	Bi	S	Total	S-Vac	Zn/(Zn+Fe)	Ag/(Ag+Cu)
1	Mg-18	Rozhd-(Fe)	wt %	43.53	6.25	1.88	3.61	–	0.08	24.92	–	–	17.97	98.24		0.31	0.80
			apfu	8.07	1.97	0.57	1.29		0.01	4.09			11.21		1.79		
2 f	Mg-3	KAgTd-(Zn)	wt %	39.16	10.47	5.55	0.05		–	24.24	–	–	19.68	99.15		0.99	0.69
			apfu	7.15	3.24	1.67	0.02			3.92			12.09		0.91		
3	Mg-18	KAgTd-(Fe)	wt %	38.81	10.96	1.54	3.92		–	24.69	–	–	18.65	98.57		0.25	0.68
			apfu	6.95	3.33	0.45	1.36			3.92			11.23		1.77		
4 i	Mg-3	KAgTd-(Zn)	wt %	37.35	11.11	5.25	0.07		–	25.54	–	–	19.28	98.60		0.98	0.66
			apfu	6.82	3.44	1.58	0.02			4.13			11.84		1.16		
5 **	Mg-6	AgTd-(Fe)	wt %	36.88	11.28	2.79	3.17	0.06	–	24.79	0.08	0.09	20.90	100.03		0.43	0.66
			apfu	6.64	3.44	0.83	1.10	0.01		3.95	0.02	0.01	12.66		0.34		
6	Mg-18	KAgTd-(Fe)	wt %	34.38	15.51	1.51	4.88		–	24.28	–	–	18.16	98.72		0.21	0.57
			apfu	5.84	4.47	0.42	1.60			3.66			10.39		2.61		
7 f	Mg-3	KAgTd-(Zn)	wt %	34.22	13.11	6.68	0.11		–	25.27	–	–	20.22	99.66		0.98	0.61
			apfu	6.07	3.95	1.96	0.04			3.97			12.08		0.92		
8 d	Mg-1	KAgTd-(Zn)	wt %	33.65	13.92	6.57	0.33		–	25.46	–	–	19.67	99.58		0.94	0.59
			apfu	5.90	4.14	1.90	0.11			3.95			11.60		1.40		
9	Mg-2	KAgTd-(Fe)	wt %	33.62	14.14	3.12	3.21		–	25.12	0.08	0.09	20.44	99.88		0.45	0.58
			apfu	5.88	4.20	0.90	1.08			3.90	0.02	0.01	12.04		0.96		
10 *	Mg-1	KAgTd-(Zn)	wt %	33.47	13.86	6.94	0.16	0.11	–	25.96	–	0.07	20.37	100.93		0.97	0.59
			apfu	5.83	4.10	2.00	0.05	0.01		4.01		0.01	11.94		1.06		
11 g		KAgTd-(Zn)	wt %	33.23	13.78	6.54	0.19	0.20	–	25.96	0.08	0.07	20.34	100.39		0.97	0.59
			apfu	5.84	4.11	1.90	0.06	0.02		4.04	0.02	0.01	12.03		0.97		
12	Mg-2	KAgTd-(Fe)	wt %	33.11	14.41	1.04	5.36	0.08	–	25.11	0.24	0.12	20.65	100.21		0.14	0.58
			apfu	5.73	4.24	0.30	1.79	0.01		3.85	0.06	0.01	12.03		0.97		
13 *	Mg-1	KAgTd-(Zn)	wt %	31.38	14.84	7.00	0.08	0.11	–	26.20	–	0.06	20.89	100.55		0.99	0.55
			apfu	5.48	4.40	2.02	0.03	0.01		4.06		0.01	12.28		0.72		
14 *		AgTd-(Zn)	wt %	29.44	16.74	6.67	0.10	0.06	–	26.12	–	0.07	21.62	100.82		0.98	0.51
			apfu	5.10	4.93	1.91	0.03	0.01		4.01		0.01	12.61		0.39		
15 g		AgTd-(Zn)	wt %	27.24	17.57	6.71	0.23	0.06	–	26.21	–	0.07	21.39	99.49		0.96	0.48
			apfu	4.74	5.19	1.93	0.08	0.01		4.04		0.01	12.54		0.46		
16 **	Mg-6	AgTd-(Zn)	wt %	26.83	17.79	6.90	0.11	–	–	26.16	0.21	0.11	22.43	100.53		0.98	0.47
			apfu	4.66	5.24	1.98	0.04			4.02	0.05	0.01	13.10		0		
17 **		KAgTd-(Fe)	wt %	26.21	20.10	3.22	3.33	0.06	–	25.72	0.09	0.09	22.02	100.84		0.45	0.43
			apfu	4.41	5.74	0.90	1.08	0.00		3.84	0.02	0.01	12.47		0.53		
18		KAgTd-(Zn)	wt %	22.91	21.54	6.87	0.30	0.16	–	26.15	0.18	–	21.93	100.02		0.95	0.39
			apfu	3.86	6.16	1.91	0.10	0.01		3.91	0.04		12.44		0.56		

Table 1　(continued)

Fahlore

Coexisting with Ag-sulfosalts (pyrargyrite, miargyrite, diaphorite, stephanite)

An. no	Sample	Mineral	Content (wt % / apfu)										Total	S-Vac	Zn/(Zn+Fe)	Ag/(Ag+Cu)
			Ag	Cu	Zn	Fe	Pb	Sn	Sb	As	Bi	S				
19	Mg-130	AgTd-(Zn)	19.72	23.98	5.53	1.65	–	–	23.92	0.15	0.08	23.31	98.33		0.74	0.33
			3.35	6.92	1.55	0.54	–	–	3.60	0.04	0.01	13.33		0		
20	Mg-6	AgTd-(Zn)	18.70	24.06	6.81	0.21	0.07	–	27.70	0.09	0.14	23.03	100.80		0.97	0.31
			3.12	6.81	1.87	0.07	0.01	–	4.09	0.02	0.01	12.92		0.08		
21	Mg-130	Ag-Tn-(Zn)	13.68	30.65	6.39	1.41	0.06	–	11.69	9.09	0.09	25.44	98.50		0.80	0.21
			2.14	8.12	1.65	0.42	0.00	–	1.62	2.04	0.01	13.36		0		

Coexisting with sulfides without Ag-sulfosalts

An. no	Sample	Mineral	Content (wt % / apfu)										Total	S-Vac	Zn/(Zn+Fe)	Ag/(Ag+Cu)
			Ag	Cu	Zn	Fe	Pb	Sn	Sb	As	Bi	S				
22	Mg-18	Rozhd-(Fe)	43.49	6.58	1.44	3.43	–	0.21	24.15	–	–	18.85	98.15		0.26	0.80
			8.18	2.10	0.45	1.25	–	0.04	4.03	–	–	11.93		1.07		
23	Mg-11	KAgTd-(Fe)	37.06	12.01	2.55	3.23	0.75	0.77	23.41	–	–	18.43	98.21		0.40	0.65
			6.66	3.66	0.76	1.12	0.07	0.13	3.73	–	–	11.14		1.86		
24	Mg-18	KAgTd-(Fe)	36.31	12.36	1.94	4.13	–	–	24.70	–	–	19.10	98.54		0.29	0.63
			6.43	3.72	0.57	1.41	–	–	3.88	–	–	11.38		1.62		
25 b	Mg-8	KAgTd-(Zn)	34.01	11.54	4.64	1.95	0.08	0.18	26.60	–	–	19.19	98.19		0.67	0.63
			6.14	3.54	1.38	0.68	0.01	0.03	4.25	–	–	11.66		1.34		
26 d	Mg-1	KAgTd-(Zn)	31.48	14.83	6.37	2.04	–	0.07	25.65	–	–	20.28	100.73		0.73	0.56
			5.37	4.29	1.79	0.67	–	0.01	3.88	–	–	11.64		1.36		
27 c	Mg-4	KAgTd-(Zn)	29.66	17.62	6.35	0.32	–	–	25.61	–	–	18.98	98.54		0.94	0.50
			5.08	5.13	1.80	0.11	–	–	3.89	–	–	10.94		2.06		
28 a	Mg-2	KAgTd-(Zn)	29.07	16.42	6.26	0.51	0.08	–	26.00	0.07	0.09	20.93	99.50		0.91	0.51
			5.08	4.87	1.81	0.17	0.01	–	4.03	0.02	0.01	12.31		0.69		
29	Mg-18	KAgTd-(Fe)	28.34	18.44	3.00	5.53	–	–	24.06	–	–	18.77	98.14		0.32	0.48
			4.69	5.19	0.82	1.77	–	–	3.53	–	–	10.46		2.54		
30 e	Mg-1	KAgTd-(Zn)	28.10	18.45	4.48	1.93	–	–	25.91	–	–	20.40	99.27		0.66	0.47
			4.81	5.36	1.26	0.64	–	–	3.93	–	–	11.75		1.25		
31	Mg-9	KAgTd-(Zn)	25.99	21.91	5.71	0.17	–	–	25.20	–	–	20.62	99.60		0.97	0.41
			4.37	6.25	1.58	0.06	–	–	3.75	–	–	11.65		1.35		

Sulfides and sulfosalts

An. no	Sample	Mineral	Content, wt %										Total	Formula
			Ag	Cu	Zn	Fe	Pb	Sn	Sb	As	Bi	S		
32 a	Mg-2	Sp	0.07	0.09	65.93	0.06						31.93	98.74	$(Zn_{1.00}Cd_{0.01})S_{0.99}$

Table 1 (continued)

Fahlore

Coexisting with Ag-sulfosalts (pyrargyrite, miargyrite, diaphorite, stephanite)

An. no	Sample	Mineral	Content					wt % apfu					Total	S-Vac	Zn/(Zn+Fe)	Ag/(Ag+Cu)
			Ag	Cu	Zn	Fe	Pb	Sn	Sb	As	Bi	S				
33 b	Mg-8	*Sp*	0.17	0.21	62.70	3.03	0.17	0.23	0.08			32.74	99.33	$(Zn_{0.94}Fe_{0.05})S_{1.00}$		
34 b		*Gn*	0.11	0.50	0.91	0.11	86.59	0.09	–			12.65	100.96	$(Pb_{1.00}Zn_{0.03}Cu_{0.02})S_{0.94}$		
35 b		*Stn*	0.31	28.96	3.12	9.46	0.90	27.53	0.33			27.34	97.95	$(Cu_{2.06}Ag_{0.01})(Fe_{0.77}Zn_{0.22})Sn_{1.05}S_{3.86}$		
36 c	Mg-4	*Gn*	0.04	–	–	–	86.15	–	–			12.75	98.94	$Pb_{1.02}S_{0.98}$		
37 c		*Blg*	2.62	–	–	–	58.03	–	23.15			14.87	98.67	$(Pb_{5.84}Ag_{0.51})Sb_{3.97}S_{9.68}$		
38 d	Mg-1	*Apy*		0.04		36.46			1.64	37.51		23.50	99.14	$Fe_{1.03}(As_{0.79}Sb_{0.02})S_{1.16}$		
39 d		*Gn*	0.07	–		0.05	86.83			–	0.36	13.20	100.50	$Pb_{1.00}S_{0.99}$		
40 d		*Prg*	58.52	0.36	0.17	0.09	1.06	–	20.54			17.90	98.64	$(Ag_{2.96}Cu_{0.03})Sb_{0.92}S_{3.04}$		
41 f	Mg-3	*Prg*	59.62	0.13	0.17	0.04	–	–	21.97			17.44	99.37	$(Ag_{3.02}Cu_{0.01})Sb_{0.98}S_{2.97}$		
42 f		*Mia*	37.40	0.05	0.09	–	–	–	39.57			21.77	98.88	$Ag_{1.02}Sb_{0.96}S_{2.01}$		
43 g	Mg-1	*Df*	24.89	0.49	0.24	–	28.98	–	27.39	–	–	19.24	101.22	$(Ag_{3.06}Cu_{0.10})(Pb_{1.85}Zn_{0.05})Sb_{2.98}S_{7.95}$		
44 g		*Prg*	59.81	–	–	–	0.15	–	22.44	0.07	0.04	17.42	99.93	$Ag_{3.02}Sb_{1.00}S_{2.96}$		
45 i	Mg-3	*Sp*	0.10	–	64.70	–	0.19	–	–			33.02	98.01	$Zn_{0.98}S_{1.02}$		
46 i		*Prg*	59.06	0.61	0.40	0.04	–	–	21.32			17.46	98.89	$(Ag_{2.99}Cu_{0.05})Sb_{0.95}S_{2.97}$		
47*	Mg-1	*Prg*	56.86	0.05	–	–	0.05	–	24.40	–	–	18.05	99.41	$Ag_{2.86}Sb_{1.09}S_{3.05}$		
48*		*Mia*	37.57	0.06	0.07	–	0.06	–	39.83	–	0.10	22.05	99.74	$Ag_{1.02}Sb_{0.96}S_{2.01}$		
49*		*Df*	23.76	0.29	0.18	0.06	30.38	–	27.31	–	–	19.07	101.03	$(Ag_{2.95}Cu_{0.06})(Pb_{1.96}Zn_{0.04})Sb_{3.00}S_{7.97}$		
50**	Mg-6	*Stf*	67.55	0.17	0.04	0.06	–	0.10	15.54			16.31	99.77	$(Ag_{4.94}Cu_{0.02})Sb_{1.01}S_{4.01}$		

Note: "–", below detection limit determined by 2σ criterion. For fahlore detection limits of some elements are, wt %: 0.04 Fe, 0.05 Pb, 0.05 Sn, 0.07 As, 0.05 Bi, 0.05 Se. Cd and Hg were not determined. Te 0.06, 0.07 and 0.08 wt % (0.01 apfu) found in 9, 28 and 12 analyses respectively; Cd 0.58 and In 0.08 wt % present in 32 analysis; Se below detection limit in all submitted analyses

Minerals: *AgTd-(Zn)* and *AgTd-(Fe)* – argentotetrahedrite-(Zn), -(Fe), *KAgTd-(Zn)* and *KAgTd-(Fe)* – kenoargentotetrahedrite-(Zn), -(Fe), *Rozhd-(Fe)* – rozhdestvenskayaite-(Fe), *Ag-Tn-(Zn)* – Ag-rich tennantite-(Zn); *Prg* – pyrargyrite, *Mia* – miargyrite, *Df* – diaphorite, *Stf* – stephanite, *Sp* – sphalerite, *Gn* – galena, *Stn* – stannite, *Apy* – arsenopyrite, *Blg*—boulangerite. Analyses are given in their decreasing order of Ag (wt %) content. The symbol next to the analysis number corresponds to the letter in Fig. 2; analyses marked with * and ** are not shown in the figures in the article

thermochemist David R. Gaskell (Sack and Ghiorso 2017, p. 838).[2]

Accordingly, in this study we will attempt to address the issue of vacancy substitutions for sulfur in $(Cu,Ag)_{10}(Fe,Zn)_2Sb_4S_{13}$ fahlores from the standpoint of phase equilibrium and thermodynamics, rather than relying on the pronouncements of mineralogical "spectroscopists." An ideal dataset for this undertaking is provided by the petrological and mineral chemical studies of the sulfide ores from the Mangazeyskoye ore deposit. This deposit has fahlores that exhibits vacancies on both the octahedrally and tetrahedrally coordinated sulfur sites, the latter being previously unrecognized in the mineralogical literature. In this analysis we will demonstrate the mechanisms by which sulfur vacancies expand the stability field of fahlore relative to that of sulfur vacancy-free $(Cu,Ag)_{10}(Fe,Zn)_2Sb_4S_{13}$ fahlores and attempt to outline general conditions that must govern the concentrations of the vacancies replacing sulfur atoms on the octahedrally and tetrahedrally coordinated sites. Finally, we will explore how the sulfur vacancies are related to sulfur fugacity, concluding that fahlore has the potential to be an ideal indicator of sulfur fugacity of the fluids from which it crystallized, once a comprehensive thermodynamic model is formulated and can be calibrated based on experimental, theoretical, and further field studies.

Geology and mineralogy of the Mangazeyskoye ore deposit

Geology

The Mangazeyskoye Ag-Pb-Zn deposit is located about 400 km northeast of Yakutsk-city and 50 km north of the nearest settlement Sebyan-Kyuel' (65° 43′ 05″ N and 130° 09′ 06″ E) in Sakha (Yakutia), Russia. Its exploration history began in the mid-eighteenth century and has had several peaks in interest (Smirnov 1962; Indolev and Nevoisa 1974). About 80 ore bodies have been explored and assayed in the deposit, which covers an area of almost 150 km² (Nekrasov 2017). The deposit consists of several closely spaced (from tens to hundreds of meters) ore zones, each of which was previously considered as a separate mineral deposit (Anikina et al. 2016). The Canadian Silver Bear Resources Company (July 7, 2015) reported indicated reserves of 800 t Ag (the Ag cutoff is 909 g/t) and inferred resources of 2250 t Ag (the Ag cut-off is 457 g/t) within such a Vertikalny zone. The Mangazeyskoye Ag-Pb–Zn deposit is proposed to be a super large one containing forecast resources of 28 kt Ag of

high grade (up to 700 g/t Ag) ores (Aristov and Nekrasov 2010; Nekrasov 2017).

The Mangazeyskoye deposit is localized in the western Verkhoyansk Fold–Thrust Belt (VFTB), which extends for 2000 km with a width of 500 km along the northeastern margin of the Siberian craton. The deposit occurs at an intersection of the Nyuektame and North Tirekhtyakh deep-seated faults in thick (up to 9–11 km) Middle Carboniferous to Early Permian clastic sand–shale sequences. The sedimentary rocks have been deformed into NW-trending folds of various shapes and metamorphosed to sericite (muscovite)–chlorite grade greenschist facies. A granodiorite porphyry massif and numerous diorite, quartz-diorite, granodiorite, granodiorite-porphyry, lamprophyre dikes N-S oriented have intruded the clastic rocks. The ore bodies are hosted in sandstones under the screens of siltstone horizons that compose the core and the steep eastern limb of the asymmetric anticline fold. Two fault zones crosscut this anticline under 5°–15° to the strike of rocks. Diagonal normal–strike-slip bedding-plane dislocations accompany these zones, so that the entire system is a strike-slip duplex that controls and hosts ore bodies.

The Mangazeyskoye deposit may be considered an Ag–Pb–Zn vein deposit in clastic sedimentary rocks comparable with the large and well explored deposits of the Kokanee Range (Beaudoin et al. 1992) and Keno Hill (Boyle 1965; Lynch 1989a, b; Sack et al. 2003; Sack and Lichtner 2009, 2010) in Canada, Coeur d'Alene in the United States (White 1998; Fleck et al. 2002; Sack et al. 2002, 2005; Sack and Lichtner 2009, 2010), Freiberg in Germany (Swinkels et al. 2021), and Příbram in the Czech Republic (Beaudoin and Sangster 1992). The latter were formed primarily from metamorphic fluids under mesothermal conditions. A recent fluid inclusions and stable isotope study (Anikina et al. 2016) suggests that the Mangazeyskoye Ag–Pb–Zn veins are derivatives of an epithermal–porphyry hydrothermal–magmatic system related to intrusion and crystallization of subvolcanic felsic stocks and involvement of compositionally contrasting H_2O-CO_2-NaCl fluids of magmatic and meteoric origin with salinity of 15.4–0.8 wt % NaCl equiv. Mineral deposition was the result of fluid phase separation (boiling) and mixing at temperatures of 120 to 340 °C under pressures of 0.2–0.5 kbar.

Mineralogy

The ore bodies are cross-cutting veins, veinlets zones, mineralized breccia, and crushing zones, and stockworks that occur only in sandstone strata in the same fault zones. Ore bodies are composed of quartz, carbonates (siderite, ankerite, and calcite), sulfides (pyrite, arsenopyrite, sphalerite, galena, chalcopyrite, stannite), and sulfosalts (fahlore, boulangerite, pyrargyrite, miargyrite, stephanite, owyheeite, diaphorite,

---

[2] "If you want to know something about speciation, the last thing you should do is consult a spectroscopist. Just look at the phase diagram.".
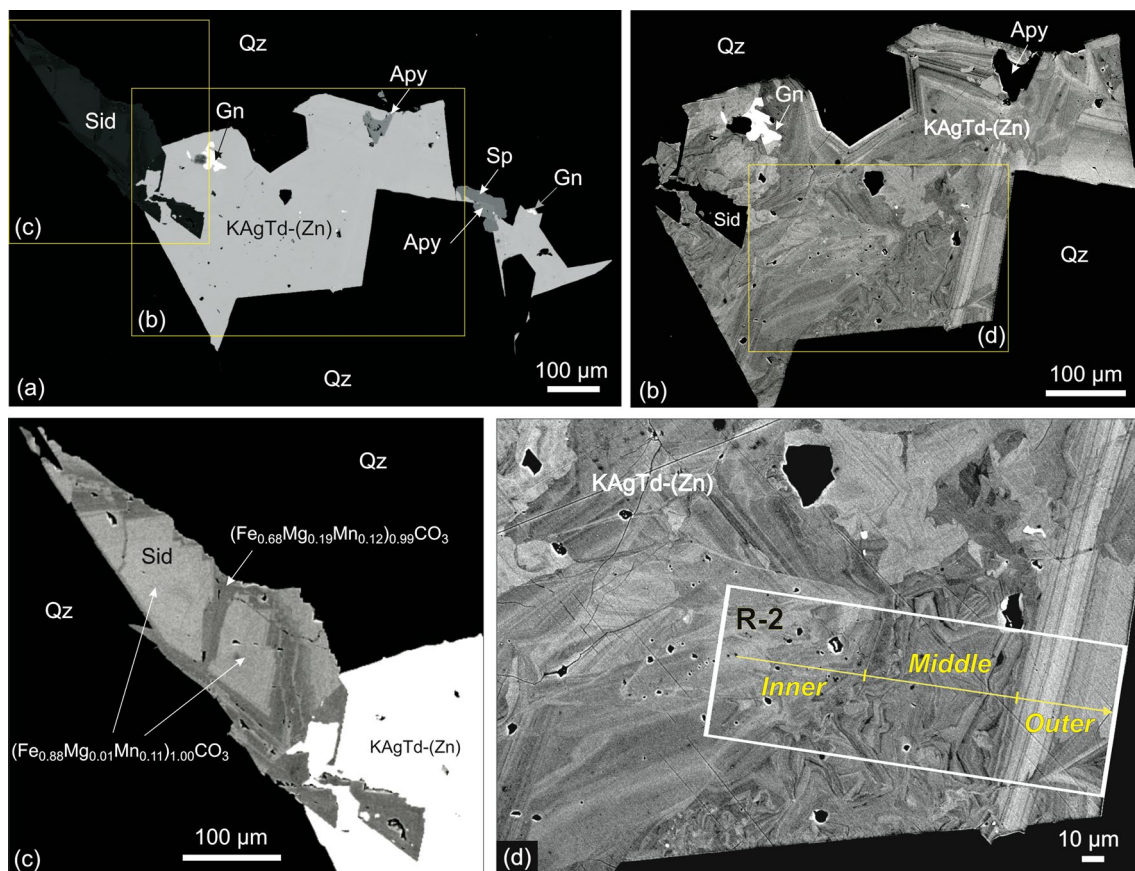
Fig. 3 BSE images showing textures and intergrowths of heterogeneous-zonal kenoargentotetrahedrite-(Zn) aggregate with sulfide and carbonate filling interstices between quartz grains in the Mangazeyskoye deposit. **a** Intergrowths of kenoargentotetrahedrite-(Zn) (KAgTd), galena (Gn), sphalerite (Sp), arsenopyrite (Apy), and siderite (Sid). **b** Heterogeneous kenoargentotetrahedrite-(Zn) aggregate with inclusions of galena, arsenopyrite, and siderite. Kenoargentotetrahedrite-(Zn) aggregate is composed of areas with unclear patchy heterogeneity and oscillatory zoning with complex interrelationships. Rhythms with fine oscillations are confined to the peripheral parts of the aggregate in contact with quartz (Qz). **c** Heterogeneous siderite aggregates in association with heterogeneous-zonal kenoargentotetrahedrite-(Zn). **d** An enlarged fragment of heterogeneous-zonal kenoargentotetrahedrite-(Zn). Yellow arrows indicate positions of R-2 EPMA profile. Normal BSE image (**a**) and BSE images with high contrast (**b**–**d**)

andorite, and freieslebenite). Massive coarse-grained, brecciated, banded, and rhythmically zoned fabrics of ores were observed. Textural and structural crosscutting and crushing relationships between mineral aggregates suggest their following depositional sequence: quartz–pyrite–arsenopyrite → quartz–carbonate–sulfide → silver–base-metal mineral assemblages. Quartz–pyrite–arsenopyrite aggregates, containing gersdorffite, wolframite, molybdenite, and Bi minerals, are accompanied by narrow greisen zones. Quartz–carbonate–sulfide aggregates are surrounded by aureoles of silicification and quartz–sericite alterations.

Silver–base-metal aggregates form the closely spaced series of thin quartz–carbonate–sulfide-sulfosalts veinlets containing Ag-rich fahlore (freibergite), boulangerite, Ag-sulfoantimonites, and Ag-Pb-sulfoantimonites. Sulfosalt minerals fill the interstices between quartz and carbonate grains. Their aggregates composed of different minerals are spatially separated and form mutual boundaries when they occur in intimate intergrowths. Such textures are consistent with the inference that they were deposited under similar physical and chemical conditions.

Fahlores occur in quartz–carbonate–sulfide ores (Figs. 2, 3), where they form mutual intergrowths with galena, pyrargyrite, miargyrite, diaphorite, sphalerite, stannite, stephanite, siderite, and arsenopyrite in interstices between quartz and carbonate grains (Fig. 2a, e, f, h, i) or contain inclusions of these minerals (Figs. 2a, d, g, i, 3a). It is often observed that fahlore corrodes quartz grains and forms pseudomorphs along the periphery of crystals (Fig. 2c). The fahlore in the deposit is often represented by zonal heterogeneous aggregates (Figs. 3b, d), which are composed of areas with unclear patchy heterogeneity and oscillatory zoning with complex relationships among themselves. Rhythms with fine

oscillations in most cases are confined to the peripheral parts of the fahlore aggregate in contact with quartz.

Samples and analysis method

Samples

Ore samples containing fahlore and associated sulfides were investigated from a collection of 10 specimens from the Mangazeyskoye deposit. A heterogeneous-zonal aggregate of argentotetrahedrite–kenoargentotetrahedrite-(Zn) was studied in sample Mg-6. This sample is a fragment of the Vasilkovskoye ore body with the highest silver grade in the deposit. It was collected on the northern flank of this ore body, opened by an exploration trench (ditch 165). This sample is matrix-supported inter-mineral breccia: angular fragments of early milky-white and gray quartz, coarse-crystalline carbonate (siderite) up to 2 cm in size infilled with sulfide galena-sulfosalt aggregates and small milled and corrosive quartz and siderite fragments in mineral flour matrix. Small voids (5–80 μm), which are filled with sulfide-sulfosalt (mainly pyrargyrite) aggregates, occur in quartz, less often in carbonate. Sulfides and sulfosalts fill microcracks in quartz and carbonate fragments. The matrix consists of fine-grained quartz, carbonate, galena, and sulfosalts: fahlore, pyrargyrite, miargyrite, and stephanite (rarely). Kenoargentotetrahedrite-(Zn) is found in intimate associations with galena, sphalerite, and other silver sulfosalts in the voids in the quartz-carbonate matrix.

Electron probe microanalysis (EPMA)

Chemical compositions of fahlore grains and zoning aggregates were studied at the Mineral Substances Analysis Laboratory at the Institute of Geology of Ore Deposits, Petrography, Mineralogy, and Geochemistry, Russian Academy of Sciences (IGEM Analytics Center for Collective Use). Microprobe analyses were obtained with a JEOL JXA-8200 SUPERPROBE with five WDS detectors operated at an accelerating voltage of 20 kV, a beam current in the Faraday cylinder of 20 nA, and a beam diameter of 1 μm, counting time of 10–20 s for major elements and 20–40 s for trace elements.

The following X-ray analytical lines: Lα for Sb, Se, Ag, As, Te, Sn; Kα for Zn, S, Cu, Fe; Mα for Hg, Bi, Pb; and Lβ for Cd were used. Synthetic compounds $AgSbS_2$ (Ag), HgS (Hg), $CuFeS_2$ (Fe), ZnS (Zn), CdS (Cd), PbS (Pb), Sb_2S_3 (Sb and S), GaAs (As), CdSe (Se), Cu_2FeSnS_4 (Sn) and pure metals Cu, Bi, and Te were used as standards. The measurements are accurate to $\pm 2\%$ rel. for major elements and ± 3–5% rel. for trace elements. ZAF corrections were calculated using the JEOL software.

Chemical compositions of fahlore were obtained using point analyses of homogenous areas and along a single line perpendicular to the zoning. The assay at points along the profile was identical to the conventional analysis. Points on the profile were selected automatically in the desired direction at a given interval with preservation throughout the X-ray focus along all the profile. The exact position of the profile's beginning and end was controlled by carbon accumulation from an electron probe. The minimum profile step (1 μm) was determined based on the size of the electron beam scattering region in the studied matrix under the above analysis conditions. A total of 188 microprobe analyses were carried out in the R-2 profile (Fig. 4) in the heterogeneous-zonal aggregate and 108 microprobe analyses were obtained in the other single grains at points.

Calculation of chemical formula of Ag-rich fahlores

Different approaches to recalculate the chemical formula of minerals belonging to the fahlore group have been described in detail (e.g., Sejkora et al. 2021a, p.721). Normalizations on the basis of $\Sigma(Me^+ + Me^{2+} + SMe^{3+}) = 16$ apfu or $\Sigma SMe = 4$ apfu are considered the most preferred when calculating the Ag-rich fahlores formula. The most common normalization based on 29 apfu for the general formula can mask some S deficiency. Therefore, when recalculating the formulas for the Ag-rich fahlores of the Mangazeyskoye deposit, normalization on the basis of $\Sigma(Me + SMe) = 16$ apfu was employed.

Fahlore chemistry

General description of the chemical composition

Representative microprobe data and calculated coefficients in formulae of fahlore are given in Table 1. The greatest variations in the Ag, Cu, Zn, Fe, and S contents in wt % are: from 17.90 to 43.53 Ag, from 6.25 to 25.51 Cu, from 1.04 to 7.16 Zn, from b.d.l.[3] to 5.53 Fe, and from 17.97 to 23.85 S (number of analyses, $n = 107$). They are nearly a pure antimony member containing from 21.38 to 27.70 wt % Sb, and minor concentration of As from b.d.l. to 1.72 wt %. A single analysis corresponds to *Ag-rich tennantite-(Zn)*[4] with 0.44 Sb/(Sb + As) and 0.21 Ag/(Ag + Cu) ratios (see Table 1, analysis 21). The amount of other minor elements

---

[3] b.d.l. – below detection limit. Detection limits for some elements are given below table 1.

[4] Here and below minerals and series of fahlore minerals are named according to the Biagioni et al. (2020) nomenclature of tetrahedrite group minerals.
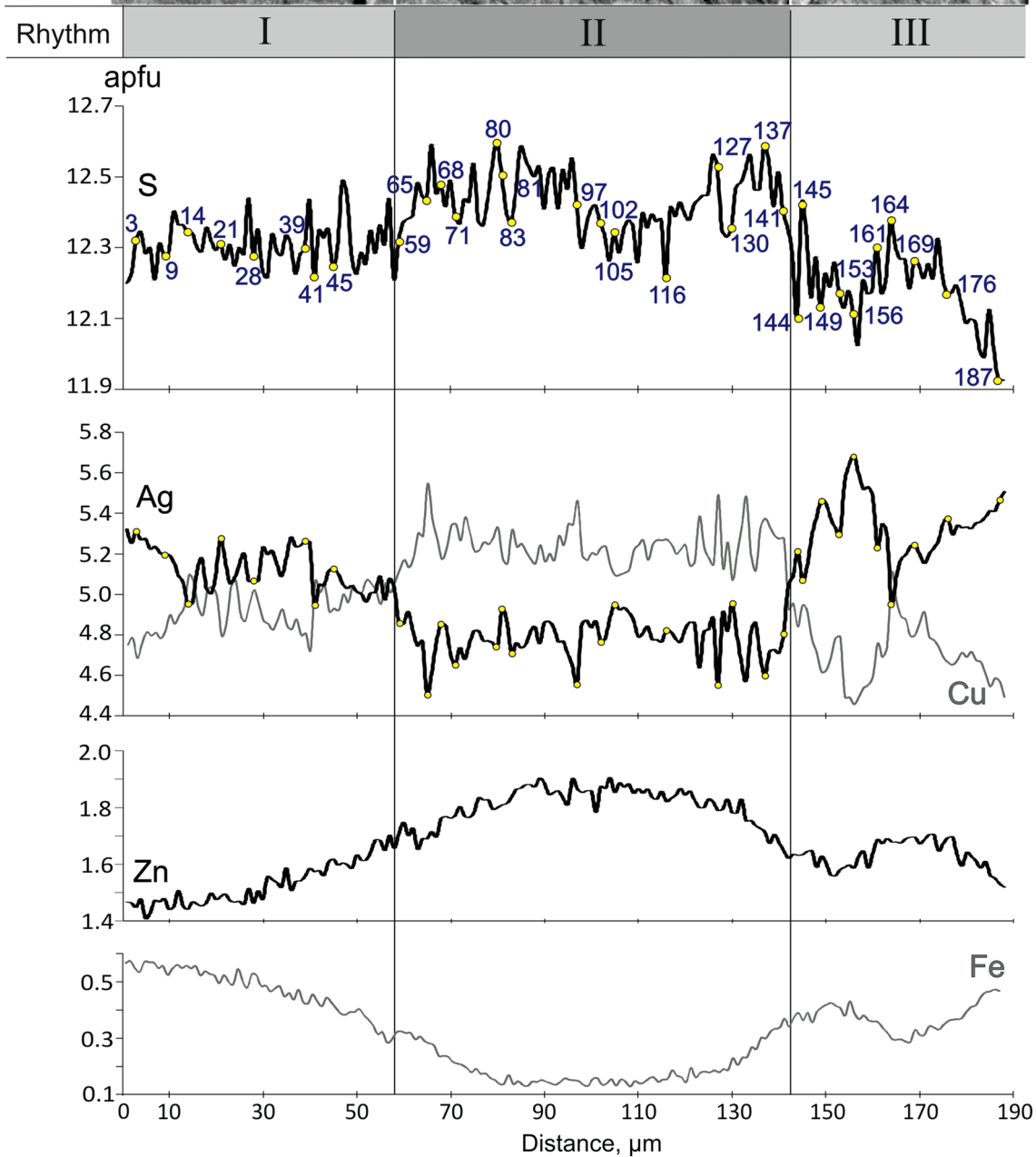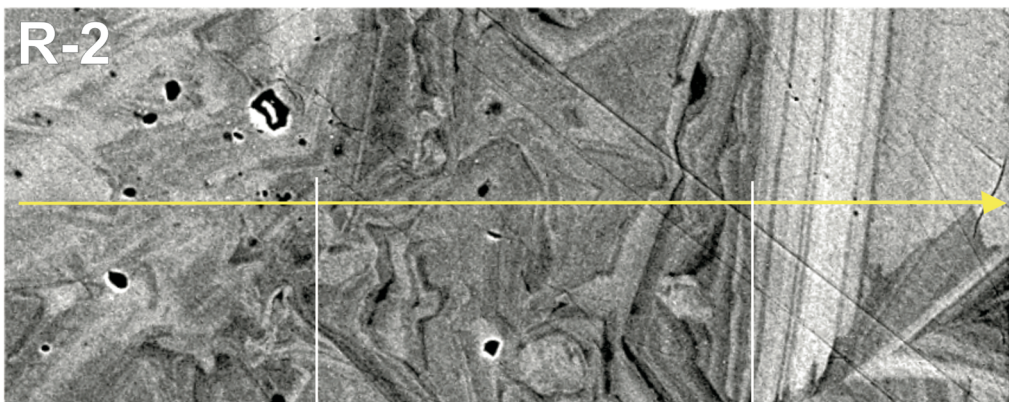
◀**Fig. 4** BSE image and compositional profiles illustrating heterogeneous-zonal aggregate of argentotetrahedrite-kenoargentotetrahedrite-(Zn) and variations in the S, Ag, Cu, Fe, and Zn contents (apfu) along the R-2 profile from Mg-6 sample (based on 188 microprobe analyses with a step of 1 μm). Point numbers on S content profile correspond to analysis numbers in Table 2. The composition curves for Sb and As are not shown, because they lack fluctuations, since the fahlore is predominately Sb-bearing with negligible As. Other minor elements are also not displayed, because their concentrations are also negligible. It appears that the temperatures of crystallization of fahlores in at least the outer rhythm III of profile R-2 were at epithermal temperatures below those at which solid state diffusion would wipe out the sharp compositional gradients between successive fahlores. This inference is supported by the experimental studies of Sack and Loucks (1985), Sack and Ebel (1993) and others, and by petrologic studies such as those Sack et al. (2002), Sack and Goodell (2002), Chincilla et al. (2016) and Zhai et al. (2019)

usually determined in the samples studied is low, wt %: up to 0.20 Bi, up to 0.77 Sn, up to 0.75 Pb, and up to 0.13 Te. A spectacular feature of some of the fahlores of the deposit is an extremely high Ag content up to ~44 wt % (Table 1, analyses 1 and 22), comparable with the highest concentration of this metal (from ≥ ~44 wt % to up to ~55 wt %) found in fahlores from a few other localities (cf. Welch et al. 2018; Biagioni et al. 2020).

The formulae calculated from the analyses do not usually correspond to the stoichiometric formula $(Cu,Ag)_{10}(Fe,Zn)_2$ $(Sb,As)_4S_{13}$ generally accepted in mineralogical textbooks. Formulae calculated based on $\Sigma(Cu + Ag + Fe + Zn + Sb + As) = 16$ atoms per formula unit (apfu) range from 2.96 to 8.18 Ag, from 1.97 to 7.28 Cu, from 0.30 to 2.04 Zn, from 0 to 1.79 Fe, from 3.19 to 4.25 Sb, from 0 to 0.42 As, and from 10.39 to 13.50 S. The total of $\Sigma Me^+_{(Cu + Ag)}$, $\Sigma Me^{2+}_{(Fe + Zn)}$ and $\Sigma SMe^{3+}_{(As + Sb)}$ varied from 9.35 to 10.61, from 1.61 to 2.72, and from 3.53 to 4.25, respectively, deviating from the stoichiometric values. Such deviation has been found by many researchers but are typically ignored in the mineralogical literature. The most remarkable finding is that the S content does not typical correspond to 13 apfu.

The EPMA studies revealed that fahlores from the Mangazeyskoye deposit belong mainly to the *freibergite series* with 0.86–1.00 Sb/(Sb + As) ratio and 2.96–7.15 Ag apfu (Table 1, Fig. 5a) and 2 analyses belong to the *rozhdestvenskayaite series* with a Sb/(Sb + As) ratio of 1.00 and 8.07–8.18 Ag apfu (Table 1, analyses 1 and 22) (Fig. 5a). A solid solution with continuous Zn–Fe and Ag–Cu substitutions exists in this freibergite series: the Zn/(Zn + Fe) ratio varies from 0.14 to 1.00 and the Ag/(Ag + Cu) ratio ranges from 0.30 to 0.69 (Figs. 5a, c). There is no correlation between the Sb/(Sb + As) and Zn/(Zn + Fe) ratios. A relationship between the contents of Ag/(Ag + Cu) and Zn/(Zn + Fe) ratios has also not been established, but it is noteworthy that Fe predominates over Zn in fahlores with highest Ag content (Fig. 5c). It is very important that there is a negative correlation between Ag and S contents (Fig. 5a).

Fahlores with a predominance of Zn over Fe prevail in the samples studied.

Previously, two generations of fahlore were reported at the Mangazeyskoye deposit (Anikina et al. 2016). The first generation included "tetrahedrite" with an Ag content of less than 6.2 wt % and a Zn/(Zn + Fe) ratio of 0.8–1.0 (according to the new nomenclature it is *Ag-rich tetrahedrite-(Zn)*), which was found intergrown with galena in quartz–carbonate–sulfide aggregates. The second generation, found in intergrowths with galena, sphalerite, and Ag-sulfosalts, is represented by "freibergite," the composition of which is as follows (wt %): 17.0–50.0 Ag, 0.1–24.8 Cu, 0.0–5.2 Fe, 0.1–7.7 Zn, 23.6–27.9 Sb; Zn/(Zn + Fe) ratio between 0.1 and 1.0, but with Zn predominating over Fe in most analyses. The Sb/(Sb + As), Zn/(Zn + Fe) and Ag/(Ag + Cu) ratios and the absence of correlation between Zn/(Zn + Fe) and Ag/(Ag + Cu) in fahlores obtained in this study are consistent with the data (Anikina et al. 2016). However, sulfur deficiency in the analyses of fahlore of the Mangazeyskoye deposit has not been previously reported.

According to the new nomenclature (Biagioni et al. 2020) five mineral types of Ag-rich fahlores were found in the samples studied. They are *kenoargentotetrahedrite–(Zn), kenoargentotetrahedrite–(Fe), argentotetrahedrite–(Fe), argentotetrahedrite–(Zn),* and *rozhdestvenskayaite-(Fe)*[5] (Fig. 5a, c; Table 1). Kenoargentotetrahedrite–(Zn) greatly predominates over other members of the tetrahedrite group (Fig. 5a, c). However, the discovery of new unapproved members of the tetrahedrite (i.e., fahlore) group, the determination of approved members and separating them from each other does not bring us one iota closer to understanding crystal chemistry and the formation conditions of fahlore in the deposit. This means that the nomenclature of tetrahedrite group minerals approved by the Commission on New Minerals of the International Mineralogical Association is "stillborn," useless and will not be used in the analysis of petrogenesis based on methods of the physical sciences.

Chemical heterogeneity and zoning in aggregates and grains of fahlore

A characteristic property of the samples studied is heterogeneity and zoning in aggregates and grains of fahlore. These are most clearly visible in BSE images: the lighter the mineral, the higher the Ag content, and vice versa, the darker the mineral, the higher the Cu content. In this aggregate, one can distinguish heterogeneous rhythms and rhythms with oscillatory zoning with complex relationships. Rhythms with

---

[5] Presumably, the occurrence of rozhdestvenkayaite-(Fe) can be identified based on two microprobe analyses (table 1, analyses 1 and 22).
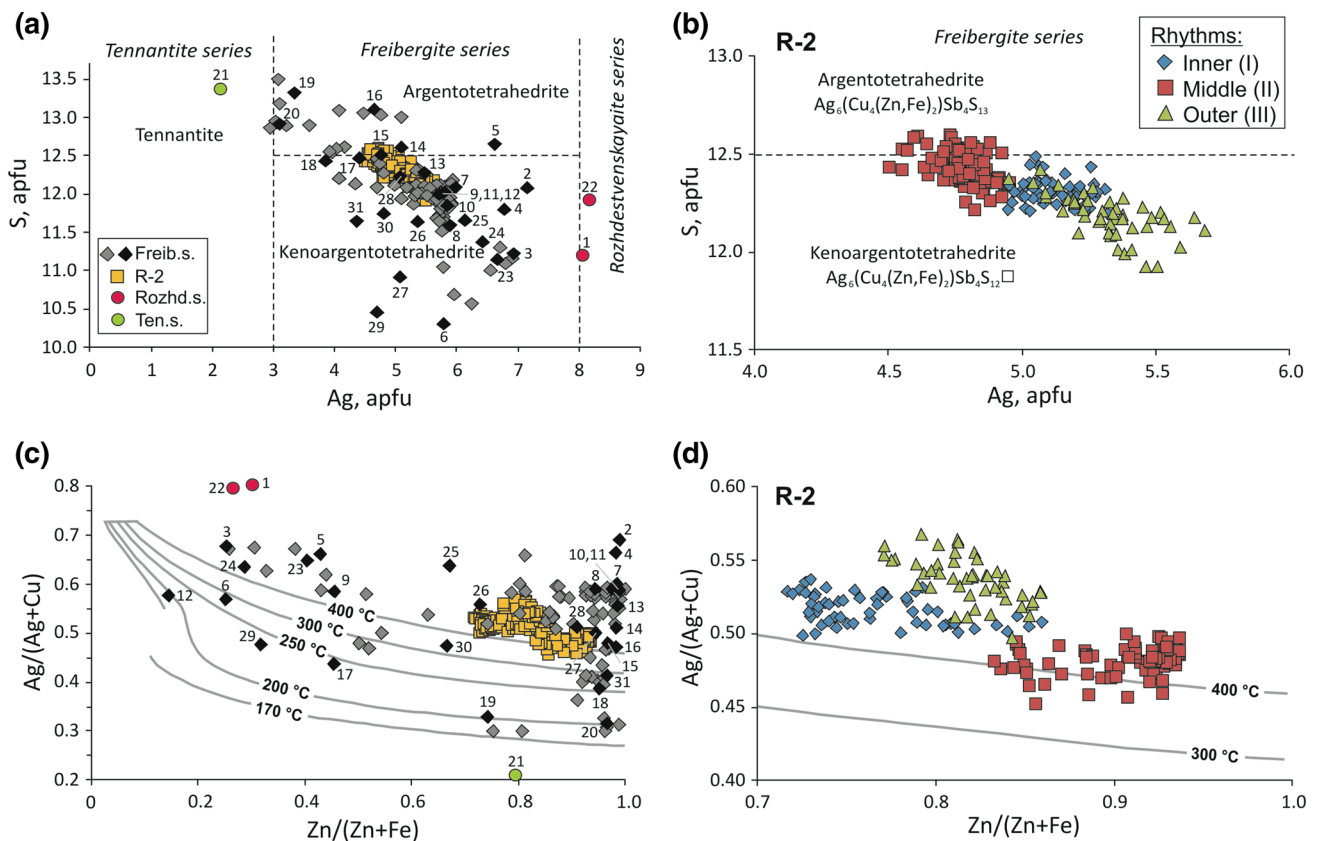
Fig. 5 Chemical composition of fahlores from the Mangazeyskoye deposit (**a, c**) and heterogeneous-zonal kenoargentotetrahedrite-(Zn) aggregates along the R-2 profile (**b, d**). **a, b** S vs Ag (apfu). Dotted lines show the boundaries between mineral species and series (Biagioni et al. 2020). **c, d** Ag/(Ag + Cu) vs Zn/(Zn + Fe). Isotherms taken from Sack (2005, Fig. 1 here). Numbers indicate the analyses given

in Table 1. It will be subsequently shown that the scatter in Fig. 5a, c is primarily related to sulfur vacancy content and secondarily to temperature. Although the fahlores in the Outer Rhythm III of profile R-2 are clearly outside the epithermal field on Fig. 5d, this inconsistency is readily resolved when the energetic consequences of sulfur vacancies are accounted for (cf. Fig. 9b)

fine oscillations are in most cases confined to the peripheral parts of the fahlore aggregate in contact with quartz. The heterogeneous-zonal aggregate of fahlore intergrown with galena, sphalerite, arsenopyrite, and zoned siderite was examined with microprobe step-traverse analyses (Fig. 4). The R-2 profile crosses a heterogeneous aggregate of fahlore (Fig. 3d), which differs in pattern (structure) and chemical composition. Rhythm I is distinguished, in which oscillatory zoning with blurred and jagged zone boundaries (pattern resembles a veil) is found in the fahlore; rhythm II with tracery (pattern looks like folds in clothes), possibly consisting of small grains of fahlore with oscillatory zoning; rhythm III, where oscillatory zoning is well manifested with rectilinear sharp boundaries between zones.

It appears that the temperatures of crystallization of fahlores in at least the outer rhythm III of profile R-2, and probably also inner rhythm I and intermediate rhythm II, were at epithermal temperatures below those at which solid state diffusion would wipe out the sharp compositional gradients between successive fahlores. The preservation of

the structure of the heterogeneous-zonal aggregate is probably due to the low diffusion rate in the solid at such low temperatures, even in the presence of a hydrothermal fluid. This inference is supported by the experimental studies of Sack and Loucks (1985), Sack and Ebel (1993) and others and by petrologic studies such as those Sack et al. (2002), Sack and Goodell (2002), Chincilla et al. (2016) and Zhai et al. (2019). A low rate of diffusion between Ag and Cu may be due to the peculiarities of the passage of a large Ag cation through the crystal lattice and through intergranular spaces (Butrymowicz et al. 1974). It was shown in Grove et al. (1984) that even at high temperatures, the oscillatory zones found in plagioclase of granodiorite plutons are preserved due to limiting of diffusion on the submicron scale. Preservation of the structure can also be associated with slow fluid seepage through small cavities between grains and along cracks in early mineral aggregates, as well as low dissolution rates of previously deposited minerals (Lyubimtseva et al. 2020).

Table 2 Representative microprobe analyses of heterogeneous-zonal argentotetrahedrite-kenoargentotetrahedrite-(Zn) along the R-2 profile (selection from 188 analyses)

An. no	Content, wt %								Total	Formula	Zn/(Zn+Fe)	Ag/(Ag+Cu)	S-Vac
	Ag	Cu	Zn	Fe	Sb	As	Bi	S					
3	30.42	15.45	5.02	1.59	26.59	–	0.11	20.98	100.21	$(Ag_{5.31}Cu_{0.69})_{\Sigma6.0}(Cu_{3.89}Zn_{1.45}Fe_{0.54})_{\Sigma5.87}(Sb_{4.11}As_{0.01}Bi_{0.01})_{\Sigma4.13}S_{12.32}$	0.73	0.54	0.68
9	29.68	15.82	5.12	1.60	26.09	0.10	0.07	20.85	99.42	$(Ag_{5.19}Cu_{0.81})_{\Sigma6.0}(Cu_{3.89}Zn_{1.48}Fe_{0.54}Cd_{0.01})_{\Sigma5.92}(Sb_{4.04}As_{0.02}Cd_{0.01})_{\Sigma4.07}S_{12.27}$	0.73	0.53	0.73
14	28.59	16.93	5.04	1.63	26.50	–	0.12	21.17	99.98	$(Ag_{4.95}Cu_{1.05})_{\Sigma6.0}(Cu_{3.93}Zn_{1.44}Fe_{0.54})_{\Sigma5.91}(Sb_{4.07}Bi_{0.01})_{\Sigma4.08}S_{12.34}$	0.73	0.50	0.66
21	30.24	15.81	5.16	1.43	26.10	0.07	0.13	20.97	100.00	$(Ag_{5.28}Cu_{0.72})_{\Sigma6.0}(Cu_{3.96}Zn_{1.49}Fe_{0.48}Pb_{0.01})_{\Sigma5.94}(Sb_{4.04}As_{0.02}Bi_{0.01})_{\Sigma4.07}S_{12.31}$	0.75	0.53	0.69
28	29.33	16.70	5.13	1.54	26.37	0.08	–	21.12	100.34	$(Ag_{5.07}Cu_{0.93})_{\Sigma6.0}(Cu_{3.97}Zn_{1.46}Fe_{0.51})_{\Sigma5.94}(Sb_{4.04}As_{0.02})_{\Sigma4.06}S_{12.28}$	0.74	0.51	0.72
39	30.31	15.92	5.44	1.25	26.42	–	–	21.06	100.48	$(Ag_{5.26}Cu_{0.74})_{\Sigma6.0}(Cu_{3.95}Zn_{1.56}Fe_{0.42})_{\Sigma5.93}Sb_{4.06}S_{12.30}$	0.79	0.53	0.70
41	28.47	16.72	5.49	1.32	26.49	–	0.09	20.90	99.59	$(Ag_{4.95}Cu_{1.05})_{\Sigma6.0}(Cu_{3.88}Zn_{1.57}Fe_{0.44}Pb_{0.01})_{\Sigma5.90}(Sb_{4.08}As_{0.01}Bi_{0.01})_{\Sigma4.10}S_{12.22}$	0.78	0.50	0.78
45	29.57	16.32	5.66	1.24	26.15	–	0.11	20.99	100.08	$(Ag_{5.13}Cu_{0.87})_{\Sigma6.0}(Cu_{3.93}Zn_{1.62}Fe_{0.42})_{\Sigma5.97}(Sb_{4.02}As_{0.01}Bi_{0.01})_{\Sigma4.04}S_{12.25}$	0.80	0.52	0.75
59	28.24	17.14	6.02	0.94	26.78	0.10	0.12	21.29	100.69	$(Ag_{4.86}Cu_{1.14})_{\Sigma6.0}(Cu_{3.86}Zn_{1.71}Fe_{0.31}Pb_{0.01})_{\Sigma5.89}(Sb_{4.08}As_{0.02}Bi_{0.01})_{\Sigma4.11}S_{12.32}$	0.84	0.49	0.68
65	26.28	18.71	5.97	0.86	26.71	–	0.12	21.57	100.31	$(Ag_{4.50}Cu_{1.50})_{\Sigma6.0}(Cu_{3.94}Zn_{1.69}Fe_{0.28})_{\Sigma5.91}(Sb_{4.06}As_{0.01}Bi_{0.01})_{\Sigma4.08}S_{12.43}$	0.86	0.45	0.57
68	27.93	17.23	6.15	0.69	26.27	–	0.11	21.34	99.81	$(Ag_{4.85}Cu_{1.15})_{\Sigma6.0}(Cu_{3.93}Zn_{1.76}Fe_{0.23})_{\Sigma5.92}(Sb_{4.04}As_{0.01}Bi_{0.01})_{\Sigma4.06}S_{12.48}$	0.88	0.49	0.52
71	27.04	17.95	6.25	0.64	26.86	0.08	0.17	21.42	100.43	$(Ag_{4.65}Cu_{1.35})_{\Sigma6.0}(Cu_{3.89}Zn_{1.77}Fe_{0.21})_{\Sigma5.87}(Sb_{4.09}As_{0.02}Bi_{0.01})_{\Sigma4.12}S_{12.39}$	0.89	0.47	0.61
80	27.39	17.93	6.31	0.45	26.28	0.11	0.10	21.68	100.30	$(Ag_{4.73}Cu_{1.27})_{\Sigma6.0}(Cu_{3.99}Zn_{1.80}Fe_{0.15})_{\Sigma5.94}(Sb_{4.02}As_{0.03}Bi_{0.01})_{\Sigma4.06}S_{12.60}$	0.92	0.47	0.40
81	28.32	17.23	6.30	0.40	26.08	–	0.08	21.37	99.87	$(Ag_{4.93}Cu_{1.07})_{\Sigma6.0}(Cu_{4.02}Zn_{1.81}Fe_{0.13})_{\Sigma5.96}(Sb_{4.02}As_{0.01}Bi_{0.01})_{\Sigma4.04}S_{12.50}$	0.93	0.49	0.50
83	27.37	17.83	6.47	0.50	26.61	–	0.10	21.38	100.41	$(Ag_{4.71}Cu_{1.29})_{\Sigma6.0}(Cu_{3.92}Zn_{1.84}Fe_{0.16}Pb_{0.01})_{\Sigma5.93}(Sb_{4.06}As_{0.02}Bi_{0.01})_{\Sigma4.08}S_{12.37}$	0.92	0.47	0.63
97	26.50	18.36	6.58	0.44	26.64	0.07	0.08	21.49	100.17	$(Ag_{4.55}Cu_{1.45})_{\Sigma6.0}(Cu_{3.90}Zn_{1.87}Fe_{0.15})_{\Sigma5.92}(Sb_{4.06}As_{0.02}Bi_{0.01})_{\Sigma4.09}S_{12.42}$	0.93	0.46	0.58
102	27.84	17.61	6.63	0.47	26.80	–	0.08	21.47	100.98	$(Ag_{4.77}Cu_{1.23})_{\Sigma6.0}(Cu_{3.89}Zn_{1.87}Fe_{0.15})_{\Sigma5.91}(Sb_{4.07}As_{0.01}Bi_{0.01})_{\Sigma4.09}S_{12.37}$	0.92	0.48	0.63
105	28.55	16.93	6.48	0.45	26.16	0.11	0.13	21.16	100.05	$(Ag_{4.95}Cu_{1.05})_{\Sigma6.0}(Cu_{3.93}Zn_{1.85}Fe_{0.15}Pb_{0.01})_{\Sigma5.94}(Sb_{4.02}As_{0.03}Bi_{0.01})_{\Sigma4.06}S_{12.34}$	0.93	0.50	0.66
116	28.21	17.69	6.46	0.45	26.71	0.08	0.08	21.25	101.04	$(Ag_{4.82}Cu_{1.18})_{\Sigma6.0}(Cu_{3.95}Zn_{1.82}Fe_{0.15}Pb_{0.01})_{\Sigma5.93}(Sb_{4.04}As_{0.02}Bi_{0.01})_{\Sigma4.07}S_{12.21}$	0.92	0.48	0.79
127	26.48	18.53	6.31	0.55	26.55	0.08	0.11	21.67	100.29	$(Ag_{4.55}Cu_{1.45})_{\Sigma6.0}(Cu_{3.95}Zn_{1.79}Fe_{0.18})_{\Sigma5.92}(Sb_{4.04}As_{0.02}Bi_{0.01})_{\Sigma4.07}S_{12.53}$	0.91	0.46	0.47
130	28.67	16.92	6.25	0.55	26.78	–	0.11	21.25	100.56	$(Ag_{4.95}Cu_{1.05})_{\Sigma6.0}(Cu_{3.91}Zn_{1.78}Fe_{0.18})_{\Sigma5.87}(Sb_{4.10}As_{0.01}Bi_{0.01})_{\Sigma4.12}S_{12.35}$	0.91	0.50	0.65
137	26.41	17.94	5.96	0.88	26.37	–	0.12	21.50	99.28	$(Ag_{4.60}Cu_{1.40})_{\Sigma6.0}(Cu_{3.90}Zn_{1.71}Fe_{0.30}Pb_{0.01})_{\Sigma5.92}(Sb_{4.07}As_{0.01}Bi_{0.01})_{\Sigma4.09}S_{12.59}$	0.85	0.46	0.41
141	27.75	17.59	5.77	0.99	26.26	–	0.10	21.30	99.80	$(Ag_{4.80}Cu_{1.20})_{\Sigma6.0}(Cu_{3.97}Zn_{1.65}Fe_{0.33})_{\Sigma5.95}(Sb_{4.03}As_{0.01}Bi_{0.01})_{\Sigma4.05}S_{12.40}$	0.83	0.48	0.60
144	30.27	16.05	5.74	1.08	26.68	0.11	0.08	20.89	100.97	$(Ag_{5.21}Cu_{0.79})_{\Sigma6.0}(Cu_{3.90}Zn_{1.63}Fe_{0.36}Pb_{0.01})_{\Sigma5.90}(Sb_{4.07}As_{0.03}Bi_{0.01})_{\Sigma4.11}S_{12.10}$	0.82	0.53	0.90
145	29.13	16.42	5.69	1.14	26.16	0.09	0.12	21.23	100.02	$(Ag_{5.07}Cu_{0.93})_{\Sigma6.0}(Cu_{3.92}Zn_{1.63}Fe_{0.38})_{\Sigma5.93}(Sb_{4.03}As_{0.02}Bi_{0.01})_{\Sigma4.06}S_{12.42}$	0.81	0.51	0.58
149	31.45	15.19	5.68	1.14	26.08	–	0.11	20.74	100.48	$(Ag_{5.47}Cu_{0.53})_{\Sigma6.0}(Cu_{3.95}Zn_{1.63}Fe_{0.38})_{\Sigma5.96}(Sb_{4.02}As_{0.01}Bi_{0.01})_{\Sigma4.04}S_{12.13}$	0.81	0.55	0.87
153	30.60	15.86	5.54	1.21	26.41	–	0.11	20.92	100.69	$(Ag_{5.29}Cu_{0.71})_{\Sigma6.0}(Cu_{3.94}Zn_{1.58}Fe_{0.40})_{\Sigma5.92}(Sb_{4.05}As_{0.01}Bi_{0.01})_{\Sigma4.07}S_{12.17}$	0.80	0.53	0.83
156	32.37	14.49	5.48	1.23	25.54	–	0.10	20.50	99.76	$(Ag_{5.68}Cu_{0.32})_{\Sigma6.0}(Cu_{4.00}Zn_{1.59}Fe_{0.42})_{\Sigma6.01}(Sb_{3.97}As_{0.01}Bi_{0.01})_{\Sigma3.99}S_{12.11}$	0.79	0.57	0.89
161	30.05	15.73	5.88	1.04	26.39	–	–	21.01	100.22	$(Ag_{5.23}Cu_{0.77})_{\Sigma6.0}(Cu_{3.88}Zn_{1.69}Fe_{0.35})_{\Sigma5.92}(Sb_{4.07}As_{0.01})_{\Sigma4.08}S_{12.30}$	0.83	0.53	0.70
164	28.56	16.99	5.87	0.94	26.28	–	–	21.22	100.02	$(Ag_{4.95}Cu_{1.05})_{\Sigma6.0}(Cu_{3.95}Zn_{1.68}Fe_{0.31}Pb_{0.01})_{\Sigma5.95}(Sb_{4.04}As_{0.01})_{\Sigma4.05}S_{12.38}$	0.84	0.50	0.62
169	30.05	15.79	5.89	0.83	26.43	–	0.10	20.88	100.04	$(Ag_{5.24}Cu_{0.76})_{\Sigma6.0}(Cu_{3.92}Zn_{1.69}Fe_{0.28}Pb_{0.01})_{\Sigma5.90}(Sb_{4.09}Bi_{0.01})_{\Sigma4.10}S_{12.26}$	0.86	0.53	0.74
176	30.83	15.31	5.89	1.00	26.23	–	0.07	20.75	100.15	$(Ag_{5.37}Cu_{0.63})_{\Sigma6.0}(Cu_{3.90}Zn_{1.69}Fe_{0.34})_{\Sigma5.93}(Sb_{4.05}As_{0.01}Bi_{0.01})_{\Sigma4.07}S_{12.17}$	0.83	0.54	0.83
187	31.17	14.80	5.29	1.34	26.52	0.07	0.13	20.22	99.58	$(Ag_{5.46}Cu_{0.54})_{\Sigma6.0}(Cu_{3.86}Zn_{1.53}Fe_{0.45})_{\Sigma5.84}(Sb_{4.12}As_{0.02}Bi_{0.01})_{\Sigma4.15}S_{11.92}$	0.77	0.55	1.08

Note: "–", below detection limit; Cd – 0.08 wt % (analysis number 9); Pb – 0.06 (41, 137, 144, 169), 0.07 (21, 59), 0.08 (105, 164), 0.10 (83) and 0.11 wt % (116). Rhythm (analysis numbers): I inner 3–45, II middle 59–141, III outer 144–187. Minerals: argentotetrahedrite-(Zn) – analysis numbers 80–81, 127 and 137; kenoargentotetrahedrite-(Zn) – others. Analyses are given in their order on the R-2 profile. The numbers of analyzes in the table correspond to the numbers in Fig. 4

The results of EPMA studies of this heterogeneous-zonal aggregate showed that they consist of a solid solution of kenoargentotetrahedrite–(Zn) and argentotetrahedrite–(Zn) with 0.99–1.00 Sb/(Sb + As), 0.45–0.57 Ag/(Ag + Cu), and 0.72–0.94 Zn/(Zn + Fe) ratios (Fig. 5b, d; Table 2). The major elements contents (wt %) are variable: 26.28–32.37 Ag, 14.44–18.71 Cu, 4.89–6.72 Zn, 0.37–1.66 Fe, 25.54–26.96 Sb, b.d.l.-0.15 As, and 20.08–21.68 S ($n = 188$). The wt % of other minor elements are: up to 0.18 Bi, up to 0.16 Cd, up to 0.14 Pb, up to 0.13 Te, up to 0.08 Se, and up to 0.07 Hg. The formula describing this kenoargentotetrahedrite–argentotetrahedrite–(Zn) solid solution is ($Ag_{4.50–5.68}Cu_{4.32–5.44})_{\Sigma 9.81–10.02}(Zn_{1.41–1.91}Fe_{0.13–0.56})_{\Sigma 1.93–2.06}(Sb_{3.97–4.18}As_{0-0.04}Bi_{0-0.02})_{\Sigma 3.99–4.19}S_{11.92–12.60}$. As far as we know, this is the first finding of a fahlore solid solution of this composition.

Microprobe analyses carried out along the R-2 profile perpendicular to the zoning revealed different compositional regions and different compositional trends (Fig. 4). In the rhythm I, slight fluctuations of Ag and S are observed in the range of 4.95–5.32 apfu around an average of ~ 5.1 apfu and in the range of 12.20–12.49 apfu around an average of ~ 12.3 apfu, respectively, at a distance of 58 μm, and the lowest concentration of Zn is 1.41–1.70 apfu (0.72–0.86 Zn/(Zn + Fe) ratio) (Table 2, analyses 3–45). The rhythm II 83 μm wide is characterized by a low Ag content of 4.50–4.95 apfu and maximum S and Zn are 12.21–12.60 apfu and 1.65–1.91 apfu, respectively (0.83–0.94 Zn/(Zn + Fe) ratio) (Table 2, analyses 59–141). In the rhythm III (Table 2, analyses 144–187), the sharpest jump with fluctuations in the composition is found: an increase in the Ag content from 4.60 (Table 2, analysis 137) to 5.68 apfu (Table 2, analysis 156) and decrease in the S content from 12.59 to 12.11 apfu over a distance of 20 μm. In the rhythm III, minimum S and maximum Ag contents are found: 11.92 apfu (Table 2, analysis 187) and 5.68 apfu (Table 2, analysis 156); Zn varies from 1.52 to 1.70 (0.77 to 0.86 Zn/(Zn + Fe) ratio. The composition of the fahlore from the external rhythm (III) in contact with quartz is closest to the stoichiometric formula $Ag_6(Cu_4Zn_2)Sb_4S_{12}$ (Biagioni et al. 2020).

It should be emphasized that the Ag content has a strong negative correlation with those of Cu and S over the entire studied interval of the heterogeneous-zonal aggregate. And, of course, there is a negative relationship between oscillations of isomorphic elements Cu and Ag, and Zn and Fe.

Sulfur vacancies

As noted above, the most spectacular feature of fahlores from the Mangazeyskoye deposit are the S deficiencies in the calculated formulae of many of them. The S content does not typically correspond to 13 apfu but is significantly lower, dropping to 10.39 apfu. It has also been established that in the fahlore at the Mangazeyskoye deposit there is a decrease in the amount of S as Ag concentrations increase (Fig. 5a, b). This trend is observed both in the deposit as a whole and in heterogeneous-zonal aggregates. It should also be noted that fahlore coexisting with sulfides in assemblages lacking other Ag-sulfosalts have predominately low sulfur contents (Fig. 5a, analyses 22–27, 29–31).

Sulfur deficiencies calculated from the EPMA suggest that up to two or more vacancies substitute for sulfur in the formula unit (Fig. 6a, b) and this is particularly intriguing, because this would require that vacancies are present on both the tetrahedral and octahedral sites normally occupied by sulfur, despite that the fact they have only been reported substituting for the octahedrally coordinated sulfur (e.g., Moëlo et al. 2008; Welch et al. 2018), and that only $Ag_6Cu_4(Fe,Zn)_2Sb_4S_{12}$ fahlores, "kenoargentotetrahedrites," are recognized as approved endmember varieties (Biagioni et al. 2020).

To consider the plausibility of this assertion it is instructive to examine plots of the positive charge excesses versus sulfur vacancies of these fahlores calculated on the assumption that Ag and Cu ions, Fe and Zn ions, As and Sb ions, and S ions have charges of + 1, + 2, and + 3, and − 2 (cf. Fig. 6c, d, colored symbols). The compelling feature of these plots, when microprobe data for fahlores are recalculated on a sixteen metal + semi-metal basis, is that the vast majority of the Mangazeyskoye fahlores are within analytical uncertainty of lines with a slope + 2 with an intercept at the origin. This observation strongly suggests that the octahedral metal clusters created by vacancies on the ^{VI}S site have variable average charge with sulfur vacancy content, decreasing from + 6 for fahlores with the ideal formula $(Ag,Cu)_{10}(Zn,Fe)_2Sb_4S_{13}$ to zero for fahlores approximating the $(Ag,Cu)_{10}(Zn,Fe)_2Sb_4S_{10}$ formula. The positive charge on these clusters would then be (6—two times the number of vacancies per formula unit) or could be represented as $[(Ag, Cu)_6^{(6-2*vac)+}]$, and this inference is supported by the observation that when the charge on these clusters is computed by this formula the net charge on the formula unit is reduced to zero, consistent with charge balance (cf. Fig. 6c, d, pale pink symbols). This is in complete accord with the conclusion of Welch et al. (2018) and Biagioni et al. (2020) that in fahlores with one vacancy per formula unit the octahedral clusters have a charge of + 4 rather than the + 6 of the ideal formula, but it indicates that the charge on these clusters will continue to decrease with increasing vacancy content. Complete metallization of these clusters would be achieved for fahlores approximating the $(Ag,Cu)_{10}(Zn,Fe)_2Sb_4S_{10}$ formula with three sulfur vacancies per formula unit, as these octahedral clusters would be fully metallically bonded at this point and would form alloy
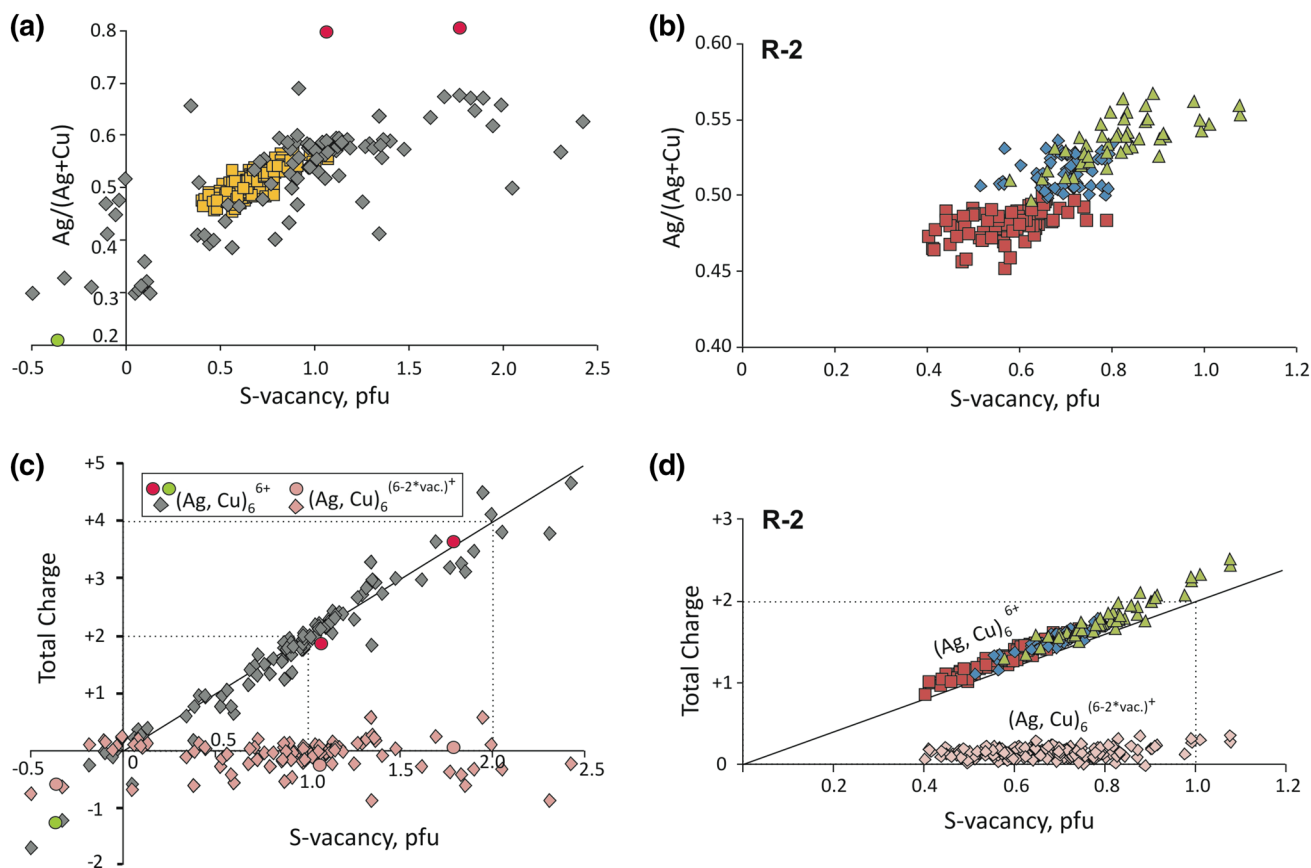
Fig. 6 Sulfur vacancies in fahlores (**a**, **c**) and in heterogeneous-zonal kenoargentotetrahedrite-(Zn) aggregate (**b**, **d**) from the Mangazeyskoye deposit. **a**, **b** Ag/(Ag + Cu) versus S-vacancy (pfu). S-vacancy calculated as 13-S (apfu) with S (apfu) calculated from microprobe analyses assuming 16 atoms of metals and semi-metals in the formula unit. **c**, **d** Total Charge versus S-vacancy (pfu). The solid line from the origin of the coordinate shows the theoretical slope of + 2 calculated for the assumption that Ag and Cu are monovalent. Colored symbols indicate total charge calculated on this basis whereas pale-pink symbols indicate total charge pfu calculated on the assumption that the charge on the octahedral metal clusters of Ag and Cu formed by removal of S from the site at the comers and center of the unit cell have an average positive charge of (6−2x(number of sulfur vacancies pfu))⁺. For designations of symbols see Fig. 5a. Negative total charges in Fig. 6c may be due to analytical uncertainties, and where both negative vacancy contents and total negative charges are calculated they may be due to inclusions of pyrite or other sulfides whose cations were not analyzed for, or stoichiometric improprieties in fahlores. In addition, since we use the formal valence of Cu and Fe ions of + 1 and + 2 to calculate the total charge, as reported in the third paragraph of the section on Sulfur Vacancies, and they may also have charges of + 2 and + 3, failure to consider the possibility that some of these ions may have these higher charges may also give negative total charges in Fig. 6c
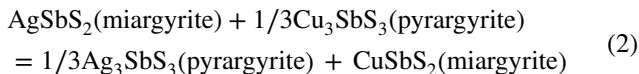
nanoparticles electrostatically unattached to the fahlore structure. Accordingly, 3 vacancies on sulfur sites per formula unit may be regarded as the intrinsic limit to vacancy content, as any further vacancy substitution for sulfur would violate ionic charge balance and lead to breakdown of the fahlore structure. The fact that Mangazeyskoye fahlores achieve calculated sulfur vacancy contents exceeding 2 pfu is consistent with the inference that the $(S)_{-1}$ substitution becomes increasingly energetically unfavorable with vacancy contents > 1 pfu, because it creates octahedral metal clusters that are less bonded by charge to the remaining structure.

Increase of fahlore Ag/(Ag + Cu) ratios due to sulfur vacancies

Despite their frequent coexistence with miargyrite, pyrargyrite, and sphalerite many of the Mangazeyskoye fahlores have Ag/(Ag + Cu) ratios much higher than those established for $(Ag,Cu)_{10}(Zn,Fe)_2Sb_4S_{13}$ fahlores coexisting with this assemblage (cf. Figure 1). This discrepancy cannot be attributed to temperature, because the temperatures required by the fahlore isotherms for $(Ag,Cu)_{10}(Zn,Fe)_2Sb_4S_{13}$ fahlores would be unrealistically high (cf. Figs. 5c, d, 9). Alternatively, this discrepancy may be readily explained by the lowering of the chemical potential of $Ag_{10}Zn_2Sb_4S_{13}$ in fahlore by sulfur vacancies.
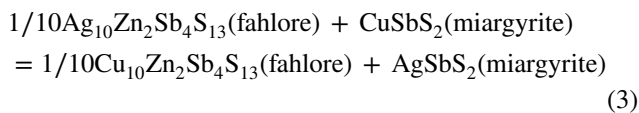
A possible method for resolving this discrepancy and estimating crystallization temperatures of Mangazeyskoye fahlores involves comparing the Mangazeyskoye fahlores data arrays with the $Ag/(Ag+Cu)$—$Zn/(Zn+Fe)$ isotherms for $(Ag,Cu)_{10}(Zn,Fe)_2Sb_4S_{13}$ fahlores coexisting with miargyrite, pyrargyrite and sphalerite calculated by Sack (2005, Fig. 1 here). The isotherms calculated by Sack (2005) are very tightly constrained for $(Cu,Ag)_{10}Zn_2Sb_4S_{13}$ fahlores by the 200–400 °C experiments of Ebel and Sack (1994) on the fahlore breakdown reaction.

$$Ag_{10}Zn_2Sb_4S_{13}(\text{fahlore}) = AgSbS_2(\text{miargyrite}) \\ + 3\,Ag_3SbS_3(\text{pyrargyrite}) + 2\,ZnS(\text{sphalerite}), \quad (1)$$
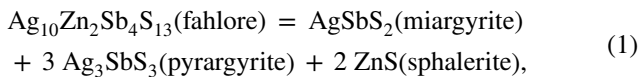
fahlores whose stoichiometry corresponds to that for the ideal stable structure with 208 valence electrons and full occupancy of the 52nd Brillouin zone (e.g., Johnson and Jeanloz 1983; Jeanloz and Johnson 1984). Sack (2005) employed these constraints on the net-transport reaction for Zn-fahlores, constraints on the Gibbs energy of formation of $AgSbS_2$ miargyrite and Ag_3SbS_3 pyrargyrite from Ag_2S and Sb_2S_3 (Schenck and von der Forst 1939; Schenck et al. 1939; Verduch and Wagner 1957), the calibrations for the Cu-Ag exchange reactions between miargyrite and pyrargyrite, and fahlore and miargyrite:

$$AgSbS_2(\text{miargyrite}) + 1/3Cu_3SbS_3(\text{pyrargyrite}) \\ = 1/3Ag_3SbS_3(\text{pyrargyrite}) + CuSbS_2(\text{miargyrite}) \quad (2)$$

and.

$$1/10Ag_{10}Zn_2Sb_4S_{13}(\text{fahlore}) + CuSbS_2(\text{miargyrite}) \\ = 1/10Cu_{10}Zn_2Sb_4S_{13}(\text{fahlore}) + AgSbS_2(\text{miargyrite}) \quad (3)$$

(e.g., Harlov and Sack 1995; Sack 2000) and the thermodynamic solution model for $(Ag,Cu)_{10}(Zn,Fe)_2Sb_4S_{13}$ fahlores of Sack (1992) to derive an expression for the Gibbs energy of formation of the $Ag_{10}Zn_2Sb_4S_{13}$ endmember component from the simple sulfides over the $170-400$ °C temperature range. He then extrapolated these results into the Fe bearing system using these Ag–Cu exchange reactions and the experimental and field constraints on the Fe-Zn exchange reaction between fahlore and $(Zn,Fe)S$ sphalerite.

$$1/2\,Cu_{10}Zn_2Sb_4S_{13}(\text{fahlore}) + FeS(\text{sphalerite}) \\ = 1/2\,Cu_{10}Fe_2Sb_4S_{13}(\text{fahlore}) + ZnS(\text{sphalerite}) \quad (4)$$
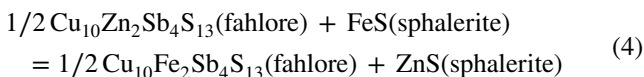
of Sack and Loucks (1985) and O'Leary and Sack (1987), and the activity—composition relations for sphalerite derived from the statistical mechanical, cluster variation method (CVM) model for $(Zn,Fe)S$ sphalerite of Balabin and Sack (2000), a model whose tenets were confirmed by the first-principle quantum mechanical calculations of

Wright and Gale (2010) and are consistent with a plethora of experimental phase equilibrium data (e.g., Arnold 1962; Barton and Toulmin 1966; Boorman et al. 1971; Scott and Barnes 1971; Scott 1973; Lusk and Ford 1978; Balabin and Urusov 1995) and the calorimetric data of Pankratz and King (1965).

The fundamental features of the calculated isotherms for $(Ag,Cu)_{10}(Zn,Fe)_2Sb_4S_{13}$ fahlores (Fig. 1) have been subsequently confirmed by the results of field studies (e.g., Lynch 1989a; Sack 2002; Sack et al. 2002, 2003; Chinchilla et al. 2016; Zhai et al. 2019; Alves et al. 2022; Zhai 2022), including the existence of the low-temperature (i.e., epithermal) miscibility gaps in these fahlores first predicted by O'Leary and Sack (1987). Accordingly, the apparent high temperatures inferred for the Mangazeyskoye fahlores from this construction (e.g., Fig. 5c, d) are difficult to rationalize, unless we account for both their octahedral and tetrahedral sulfur vacancies. In the absence of constraints on homogeneous equilibria involving these vacancies, detailed knowledge of the energetics associated with metallization of the Ag and Cu atoms surrounding the sites of the octahedral sulfur vacancies (e.g., Welch et al. 2018; Biagioni et al. 2020; this study), and other uncertainties associated with deviations from the formula for the most stable fahlores (e.g., Johnson and Jeanloz 1983; Jeanloz and Johnson 1984), some simplifying assumptions are in order.

To begin with we will assume that the deviations of $Ag/(Ag+Cu)$ ratios (i.e., X_4) of the Mangazeyskoye fahlores from those given by the construction of Sack (2005) are exclusively due to the lowering of the chemical potential of the $Ag_{10}Zn_2Sb_2S_{13}$ component in the net-transport (i.e., breakdown) reaction of fahlore to miargyrite, pyrargyrite and sphalerite. Here the issue is to what extent the $Ag/(Ag+Cu)$ ratio must be raised, or to what extent the field of fahlore must expand on the $Ag/(Ag+Cu)$—$Zn/(Zn+Fe)$ diagram at a given temperature and X_2 or $Zn/(Zn+Fe)$ ratio (i.e., Le Chatelier's principle) to restore the net-transport reaction to equilibrium. To do so in a first approximation, we will ignore the complexities of non-ideality in the vibrational Gibbs energy and of Ag–Cu ordering between trigonal-planar and tetrahedral sites and consider only the ratio of the disordered configurational component of the chemical potential of $Ag_{10}Zn_2Sb_4S_{13}$ of the sulfur vacancy-free fahlore, $RT \ln [(X_4^{\text{with no vacancies in fahlore}})^{10} (X_2)^2]$ with values of X_4 given by the calibration of Sack (2005, Fig. 1 here), and that of the vacancy substituted fahlore assuming it has only ten atoms of $Ag + Cu$ per formula unit, $RT \ln [(X_4^{\text{with vacancies}})^{10}(X_2)^2(X_S^{IV})^{12}(X_S^{VI}))$. At constant temperature and X_2, the ratio of these quantities that will satisfy the condition of equilibrium of the net-transport reaction should be close to.

$$1 = [(X4 \text{ } with \text{ } no \text{ } vacancies \text{ } in \text{ } fahlore)^{10}$$
$$/((X4 \text{ } with \text{ } vacancies)^{10}(X_S^{IV})^{12}(X_S^{VI}))], \tag{5}$$

if we ignore changes in the compositions of miargyrite, pyrargyrite, and sphalerite associated with the different values of X_4. This cannot be strictly correct, as increased X_4 will increase both the Ag/(Ag + Cu) ratios of pyrargyrite and miargyrite due to the Ag–Cu exchange reactions between fahlore and pyrargyrite and fahlore and miargyrite. But because Ag is very strongly concentrated in these minerals relative to fahlore, the positive increases in their mole fractions of Ag_3SbS_3 and $AgSbS_2$, and hence their chemicals potentials will be negligible, but they will nonetheless result in further, almost imperceptible, expansion of the fahlore stability field on the X_4–X_2 plot. In general, increasing X_4 in fahlore at constant X_2 will increase the Zn/(Zn + Fe) ratio, and hence the chemical potential of ZnS, in coexisting sphalerite due to the incompatibility between Zn and Ag in fahlore expressed by a positive Gibbs energy of the reciprocal reaction:

$$Cu_{10}Zn_2Sb_4S_{13} + Ag_{10}Fe_2Sb_4S_{13}$$
$$= Cu_{10}Fe_2Sb_4S_{13} + Ag_{10}Zn_2Sb_4S_{13}, \tag{6}$$
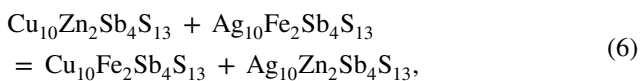
but this increase in partitioning of Fe and Zn between fahlore and sphalerite with increasing X_4 is interrupted at intermediate values of X_4 due to a change in Ag–Cu site ordering, a change that is responsible for the low-temperature (i.e., epithermal) miscibility gaps observed in natural fahlores (cf. O'Leary and Sack 1987; Sack 2017). Accordingly, we are forced to rely on the old geochemical adage that "in complex geochemical calculations the errors tend to cancel" (personal communication from H.C. Helgeson to ROS) until experimental, theoretical, and further field studies result in a satisfactory model that is as accurate as that developed for $(Ag,Cu)_{10}(Zn,Fe)_2Sb_4S_{13}$ fahlores.

We could readily determine the increases in X_4 associated with sulfur vacancy contents, if the conditions of homogeneous equilibrium relating octahedral to tetrahedral sulfur vacancies and the vibrational nonideality associated with these conditions were known. But as they are not known, we are forced to make some assumptions about the distribution of sulfur vacancies between the octahedral sites at the corners and center of the unit cell and the tetrahedral sites. Following conventional mineralogical "wisdom" we will assume that the sulfur vacancies are primarily in the octahedral sites when total sulfur vacancies do not exceed one pfu. In addition, we will make the assumptions that these vacancies are linearly related to the total sulfur vacancies until this limit is reached and that the octahedral vacancies retain the value they have at this limit (x), when total sulfur vacancies exceed it. Utilizing these assumptions, we may then determine what values of x are required to produce differences in

X_4 between those established for $(Ag,Cu)_{10}(Zn,Fe)_2Sb_4S_{13}$ fahlores and the maximum ones determined here.

To do so, it is appropriate to consider the data array defined by Zn-rich fahlores with average X_2 of about 0.95 (cf. Figs. 5c and 8), as the isotherms are tightly constrained for $(Ag,Cu)_{10}Zn_2Sb_4S_{13}$ fahlores by the experiments of Ebel and Sack (1994) and these fahlores form the most comprehensive array reported here. Assuming a temperature of about 260 °C, the value of X_4 is about 0.39 for X_2 of 0.95 in $(Ag,Cu)_{10}(Zn,Fe)_2Sb_4S_{13}$ fahlores and this corresponds quite nicely with the low X_4 end of the array, an array which extends to a maximum value of about 0.7 X_4. According to the approximations we are employing this requires a value of x slightly greater than around 0.995 to satisfy the Mangazeyskoye fahlore data (cf. Fig. 8). Noteworthy features of this diagram include the prediction that X_4 is relatively insensitive to total sulfur vacancy content up to about 0.4 vacancies pfu, achieving progressivity steeper dX_4/d slopes until total vacancies approach 1.

Although the approximation given by Eq. (5) appears to provide a reasonable first-order accounting for the functional relationship between X_4 and vacancy contents in fahlores with vacancy contents ≤ 1 pfu, it needs to be modified for vacancy contents > 1 pfu, as these fahlores do not appear to exhibit increasing X_4 with further increase in vacancy contents (cf. Figure 6a) and there may even be a maximum in X_4 around one vacancy pfu. This observation may be readily accounted for, providing we acknowledge that mixing of tetrahedrally coordinated sulfurs and vacancies may be highly nonideal and attempt to use a strictly regular solution parameter $^{IV}W_{\square-S}$ to describe this nonideality. For this assumption an appropriate approximation might be

$$RTln\left[\left(X_4^{\text{with no vacancies in fahlore}}\right)^{10}\right]$$
$$= RTln[\left(X_4^{\text{vacancies in fahlore}}\right)^{10}\left(X_S^{IV}\right)^{12}\left(X_S^{VI}\right)] \tag{7}$$
$$+ {}^{IV}W_{\square-S}\left(X_\square^{IV}\right)^2,$$

which may be written in more compact form as

$$0 = RTln[\left(X_4^{\text{with no vacancies in fahlore}}\right)^{10}/$$
$$\left(\left(X_4^{\text{with vacancies}}\right)^{10}\left(X_S^{IV}\right)^{12}\left(X_S^{VI}\right)\right)] - {}^{IV}W_{\square-S}\left(X_\square^{IV}\right)^2 \tag{8}$$

Although the $dX_4/d\square$ slope for total $\square > 1$ pfu is not well defined by the present data, $^{IV}W_{\square-S}$ must be a positive number (i.e., on the order of 50—100 kJ/gfw) to achieve the zero $dX_4/d\square$ slope shown in Fig. 8, assuming this nonideality can be adequately expressed by a strictly regular solution parameter. But a nonideality of this order is consistent with the fact that substantial replacement of tetrahedrally coordinated sulfurs with vacancies will substantially destabilize the fahlore structure leading to its collapse (i.e., breakdown)

Fig. 7 **a** (Ag + Cu) apfu versus (Sb + As) apfu of Mangazey-skoye fahlores calculated on a Σ(Me + SMe) = 16 apfu basis. Symbols are identical to those in Fig. 5 **b** Expanded version of a in section enclosed by dotted lines with horizontal and vertical lines with (Ag + Cu) = 10 and (Sb + As) = 4 indicating the stoichiometric coefficients of the metals and semimetals in the ideal fahlore formula unit. Slanted line $(Ag + Cu)_{10+x} = (Sb + As)_{4-x}$ has positive x when sulfur vacancies > 1 pfu. Numbers indicate the analyses given in Table 1
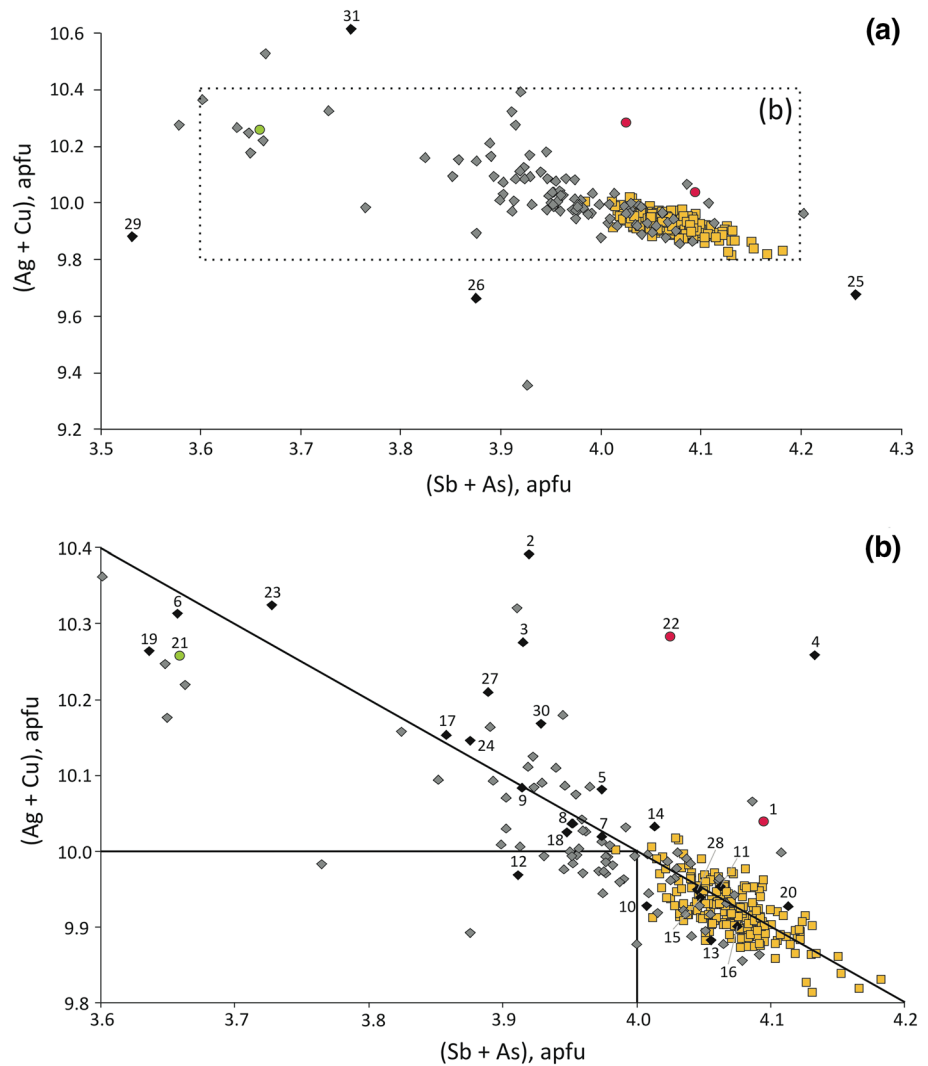
with $X_\square^{IV}$ near the upper limit inferred here ($X_\square^{IV} \sim 0.133$) for total vacancies of around 2.6 pfu. Among the minerals that would be produced by the breakdown of the fahlore component $(Ag,Cu)_{10}(Fe,Zn)_2Sb_4S_{10}$ include sphalerite, miargyrite, chalcopyrite and Ag–Cu metal alloys (e.g. Jian et al 2020), the exact proportions of these minerals being dependent on the Ag//(Ag + Cu) and Zn/(Zn + Fe) ratios of the fahlore breaking down.

Of course this treatment is clearly a simplification, particularly with regards to the adoption of the 10/4/2 (Au,Cu)/(Sb,As)/(Zn,Fe) ratio of the ideal fahlore formula unit. This is not strictly correct as illustrated in Fig. 7b where $(Ag + Cu)_{10+x} = (Sb + As)_{4-x}$ and (Zn + Fe) = 2, and $-0.2 < x < 0.4$ describes the stoichiometry of the metals and semi-metals of Mangazeyskoye fahlores to a rough approximation and (Sb + As) and (Ag + Cu) vary between about 4 to 3.6, and 10 to 10.4 with increasing $\square > 1$ pfu. Without the ability to assess the energetic consequences of such

stoichiometric improprieties (i.e., variations) at this point due to the absence of appropriate experimental investigations, we may only add them to the list of many other issues that need to be addressed (e.g., the energetics of ordering of Ag and Cu atoms between the octahedral metal clusters and those in tetrahedral metal sites, phase boundaries for breakdown of sulfur vacancy substituted fahlores as a function of temperature, etc.) before a comprehensive thermochemical model for sulfur vacancy substituted fahlores may be developed. We do note that it is fortuitous that the 10/4/2 (Au,Cu)/(Sb,As)/(Zn,Fe) ratio of the ideal fahlore formula unit appears to be a close approximation for Mangazeyskoye fahlores with 1 $\square$ pfu.

This analysis can readily be extended to more Fe-rich fahlores by adding to the X_4—X_2 diagram 200 °C and 250 °C contours obtained by solving Eq. (5) for $\square$1 pfu and x = 0.995 (e.g., Fig. 9). This exercise suggests that the Mangazeyskoyean fahlores with the maximal Ag/(Ag + Cu) ratios were crystallized at temperatures between about 260°
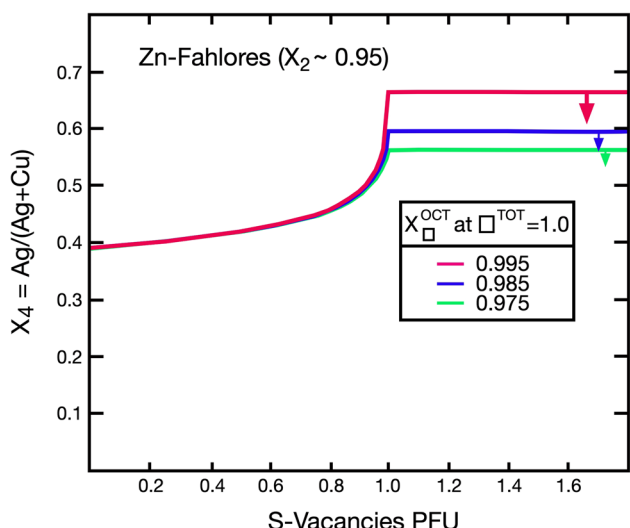
Fig. 8 Variation of X_4 ($Ag/(Ag+Cu)$) with sulfur vacancy content per formula unit for Zn-fahlores with an average X_2 ($Zn/(Zn+Fe)$) of about 0.95 utilizing the approximation given in the text (Eq. 5) for values of x (mole fractions of vacancies on octahedral sulfur sites at total vacancy content of unity pfu) of 0.975, 0.985 and 0.995. Vertical arrows attached to horizontal lines for X_4 for total vacancy content > 1 pfu indicate that X_4 may be less than the value for total vacancy content = 1 pfu (i.e., X_4 may be a maximum at the total vacancy content = 1 pfu at a given value of x)

and 230 °C. However, some of the fahlores currently reflect lower temperatures, because some of them plot below such isotherms for $(Ag,Cu)_{10}(Fe,Zn)_2Sb_4S_{13}$ fahlores, and these lower temperature fahlores have significantly lower sulfur vacancies (cf. Figure 6a). These exceptions are clearly the result of their crystallization at lower temperatures or
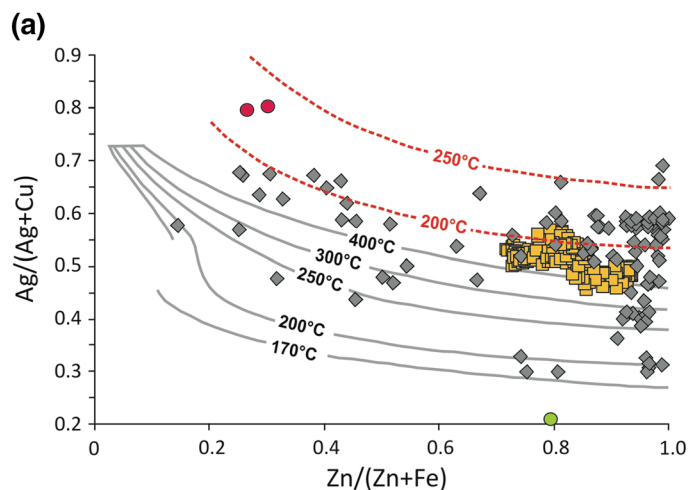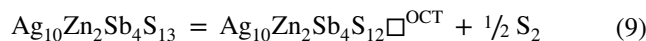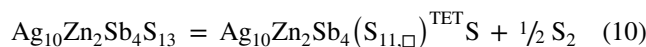
retrograde exchange with cooling. The latter possibility would not be unexpected particularly in the more Fe-rich fahlores as they are significantly less refractory than Zn-rich fahlores (cf. Sack and Loucks 1985; Sack et al. 2003) and are thus much more susceptible to retrograde exchange with cooling. Whatever the origin of these lower temperature fahlores, temperatures inferred for them from the X_4-X_2 diagram for $(Ag,Cu)_{10}(Fe,Zn)_2Sb_4S_{13}$ are in accord with the development of stephanite, a mineral whose maximum thermal stability is 197 °C (Keighin and Honea 1969) and a temperature of about 155 °C calculated from Fe-Zn partitioning between sphalerite and stannite-kesterite of the Mangazeyskoye ore deposit using the calibration of Nakamura and Shima (1982).

The main takeaway from our analysis is that fahlores from low-sulfidation environments have great potential to serve as petrogenetic indicators of sulfur fugacity through reactions such as.
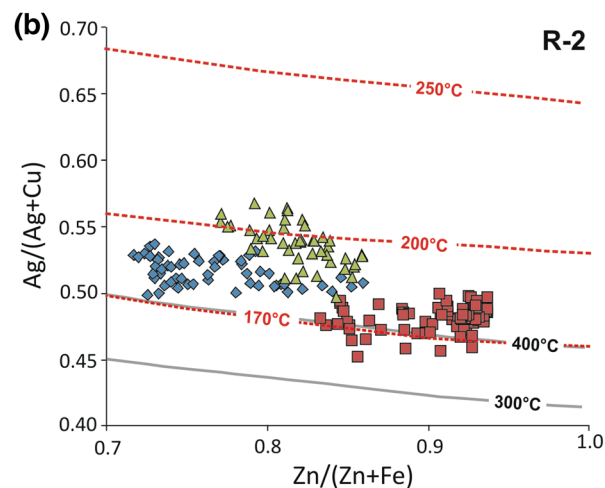
$$Ag_{10}Zn_2Sb_4S_{13} = Ag_{10}Zn_2Sb_4S_{12}\square^{OCT} + \tfrac{1}{2} S_2 \qquad (9)$$

and

$$Ag_{10}Zn_2Sb_4S_{13} = Ag_{10}Zn_2Sb_4(S_{11,\square})^{TET}S + \tfrac{1}{2} S_2 \quad (10)$$

and the homogeneous reaction given by the difference of these reactions:

$$Ag_{10}Zn_2Sb_4(S_{11,\square})^{TET}S = Ag_{10}Zn_2Sb_4S_{12}\square^{OCT} \qquad (11)$$

Of course, quantitative realization of this potential will require experimental determinations of sulfur vacancy concentration as a function of sulfur fugacity and characterization of the vibration non-idealities and atomic configurations

Fig. 9 Molar $Ag/(Ag+Cu)$ and $Zn/(Zn+Fe)$ ratios of fahlores (a) from the Mangazeyskoye deposit and (b) from the heterogeneous-zonal kenoargentotetrahedrite-(Zn) aggregates along the R-2 profile compared with the isotherms for $(Cu,Ag)_{10}(Fe,Zn)_2Sb_4S_{13}$ fahlores in the miargyrite + pyrargyrite + sphalerite assemblage (gray curves,

Sack 2005, Fig. 1 here) and those for $(Cu,Ag)_{10}(Fe,Zn)_2Sb_4S_{12}$ fahlores (**a**) at 200 and 250 °C and (**b**) at 170, 200 and 250 °C calculated with the approximation given by Eq. (5) with x = 0.995 (red dotted curves)

associated with vacancy substitutions. Lacking such information variations in X_4 in the Mangazeyskoye fahlores may only be used to define rhythmic variations in the sulfur fugacity of the hydrothermal fluids from which they crystallized.

Discussion

The observations reported here and the simplified analysis conducted to rationalize them suggest that the Mangazeyskoye sulfur vacancy-rich fahlores with the highest Ag/(Ag + Cu) ratios crystallized at temperatures between about 230 and 260 °C. This inference is the result of comparison of ratios of Ag/(Ag + Cu) and Zn/(Zn + Fe) of the most Ag-rich Mangazeyskoye fahlores with values of these ratios in fahlores with vacancy contents near 1 pfu calculated using the crude approximation given by Eq. (5) and the isotherms for $(Ag,Cu)_{10}(Zn,Fe)_2Sb_4S_{13}$ fahlores coexisting with miargyrite, pyrargyrite, and sphalerite determined by Sack (2005) (cf. Figs. 5c, 8, 9). This inference is consistent with the conclusions of Anikina et al. (2016) that tetrahedrite fahlores belong to the Ag-base metal stage of the sulfide-sulfosalt paragenetic sequence which crystallized over a temperature range of about 125–280 °C. These fahlores were thus produced near the upper temperature limits of this stage, and contrast with fahlores with lower Ag/(Ag + Cu) and vacancy contents (cf. Fig. 6a, b) which indicate lower equilibration/crystallization temperatures depending on Zn/(Zn + Fe) ratio of fahlore. Lower temperatures within this temperature range are also supported by Zn-Fe partitioning between sphalerite and stannite-kesterite and the occasional presence of stephanite in Mangazeyskoye assemblages. Based on the calibration of Nakamura and Shima (1982) a sphalerite + stannite-kesterite assemblage shown in Fig. 2b represents a temperature of about 155 °C (cf. Shimizu and Shikazono 1985) and stephanite indicates T < 197 °C, as this is the maximum temperature of its stability (Keighin and Honea 1969). And, of course, the variations of vacancy contents in rhythmically zoned fahlores from the Mangazeyskoye ore deposit are indicative of pronounced variations and repetitions in the temperatures and sulfur fugacities in the fluids from which they crystallized. Although an adequate thermodynamic model for sulfur vacancy substituted fahlores is presently unavailable to quantity the sulfur fugacity's of the parental fluids, such fahlores may be used to define their relative sulfur fugacity's and temporal variations. Such variations are apparent in the heterogeneous-zonal aggregate of argentotetrahedrite–kenoargentotetrahedrite-(Zn) fahlore (Figs. 3d, 4) where the average vacancy contents of the fahlores are highest the outermost layers (RIII), lowest in the intermediate layers (RII) and intermediate in the core (RI). The average sulfur fugacity's of the fluids from which

they crystallized were lowest for RIII, highest for RII and intermediate for RI fahlores, if the temperatures of crystallization of these fahlores were similar.

Further quantification will not be possible without the development of a reliable thermodynamic model for sulfur vacancy substituted fahlores. This will certainly be a formidable task, as such a model has not even been formulated, would require the calibration of substantially more parameters than those required for $(Ag,Cu)_{10}(Zn,Fe)_2(As,Sb)_4S_{13}$ fahlores (e.g., Sack 2017) and there are presently virtually no experimental constraints to do such a calibration. Such a development would also require that the assumption about the structural role of Ag in fahlore of the mineralogical community be revisited to conform with the precepts of thermodynamics and statistical mechanics and be consistent with the observation that low-temperature (< 200 °C) miscibility gaps exist in natural fahlores that closely approximate the $(Ag,Cu)_{10}(Zn,Fe)_2Sb_4S_{13}$ formula (e.gSack et al. 2003; Chinchilla et al. 2016; Sack 2017; Zhai et al. 2019; Alves et al. 2022; Zhai 2022). This reassessment might begin with examination of the temperature dependence of the cell edge lengths of synthetic Ag-rich fahlores as a function of annealing temperature, paralleling the studies of Ebel (1993) for $(Ag_{0.73},Cu_{0.27})_{10}Zn_2Sb_4S_{13}$ fahlore and Barton and Toulmin (1966) for Zn-Fe-S sphalerites (cf. Balabin and Sack 2000, their Fig. 6). And, of course, such a model will have to quantify the effects of the nature and compositions of octahedral Ag–Cu clusters centered on the vacated S^{VI} sites on the configurational entropy and vibrational energy and other thermodynamic properties and correctly predict the existence and compositions of the binodes of the low temperature miscibility gaps. It is also obvious that hydrothermal and/or sealed silica tube experiments at varying temperatures and sulfur fugacity's will be required to constrain sulfur vacancy forming and homogeneous reactions (9–11). Completion of these exercises should lead more realistic (i.e., lower f_{S2}) bounds on the stability field of fahlore at a given temperature than those currently calculated on an assumed 13 sulfur stoichiometry.

Despite these uncertainties, the present analysis clearly demonstrates that vacancies substitute for tetrahedrally coordinated sulfurs in fahlores in low sulfidation environments, and this $\square(S^{IV})_{-1}$ substitution must be substantially more nonideal than the $\square(S^{VI})_{-1}$ substitution to account for the apparent maximum in Ag/(Ag + Cu) ratios in fahlores near 1$\square$ pfu (cf. Figures 6a, b). For $\square$ < 1 pfu the $\square(S^{VI})_{-1}$ substitution may be substantially ideal, given that a change in the charge of the octahedral metal clusters from + 6 to + 4 is accomplished by increasing metallic bonding between nearest neighbor metal atoms. But metallization of Ag and Cu ions in the octahedral clusters becomes more energetically difficult with vacancy contents $\square$ > 1 pfu, as this requires charge imbalances over greater distances and would lead to

the production of Ag–Cu alloy nanoparticles (e.g., Jian et al. 2020) rattling around in the structure fully electrostatically unattached at the intrinsic limit of 3 sulfur vacancies pfu. It is therefore unlikely that the intrinsic limit of three sulfur vacancies pfu is ever achieved in natural fahlores, even when they break down to assemblages containing metals. And the fact that the Mangazeyskoye fahlores appear to have a limit of greater than 2 vacancies substituting for S lends credibility to the assumption that $Ag_{10}Zn_2Sb_4S_{12\square}{}^{OCT}$ and $Ag_{10}Zn_2Sb_4\,(S_{11\square})^{TET}S^{OCT}$ will be sufficient to serve as end-member fahlore vacancy components in a thermodynamic analysis.

Conclusions

Fahlores from the Mangazeyskoye Ag-Pb-Zn ore deposit have sulfur contents between about 13 and 10.4 atoms per formula unit (apfu) calculated from EPMA on the assumption that there are 16 metals and semi-metals atoms in the formula unit. Assuming the charges on the metals Ag and Cu are $+1$, those on the metals Zn and Fe are $+2$, those on the semimetals Sb and As are $+3$ and that of S is -2, these fahlores lie along lines of charge versus sulfur vacancy content with a slope of $+2$ and zero intercept within analytical uncertainty. Accordingly, if an ionic model is assumed, the charge on the octahedral Ag and Cu clusters formed by vacating the sulfur sites at the corners and center of the fahlore unit cell ($Z=2$) must be reduced from the nominal value of $+6$ to that given by the formula ($+6-2\,n\square$) if charge balance is to be preserved. This implies that the absolute intrinsic limit on vacancies that may substitute for sulfur is three pfu, as this would lead to full metallization of Ag and Cu atoms in these clusters, producing alloy nanoparticles electrostatically unattached to the remaining fahlore structure. The greater Ag/(Ag + Cu) ratios of the sulfur vacancy-rich Mangazeyskoye fahlores than those of $(Ag,Cu)_{10}(Zn,Fe)_2Sb_4S_{13}$ fahlores in equilibrium with miargyrite, pyrargyrite and sphalerite may be accounted for by equating approximations for the configurational portions of the chemical potential of $Ag_{10}Zn_2Sb_4S_{13}$ in $(Ag,Cu)_{10}(Zn,Fe)_2Sb_4S_{13}$ and vacancy substituted fahlores. Satisfactory agreement is achieved providing sulfur vacancies are nearly all on the octahedrally coordinated sulfur site when there are less than 1 sulfur vacancy pfu, and it is assumed that Mangazeyskoye fahlores with vacancy concentrations near this limit and with maximal value of Ag/(Ag + Cu) crystallized at temperatures between about 230 and 260 °C. This inference is consistent with the observations of Anikina et al. (2016) that Mangazeyskoye fahlores crystallized in the third of three depositional successions that were deposited in the 120–340 °C temperature range of petrogenesis. But some of the vacancy-poor Mangazeyskoye fahlores crystallized at temperatures nearer to the lower portion of this temperature range of petrogenesis, as reflected by their Ag/(Ag + Cu) ratios, the temperature of about 155 °C calculated from Fe-Zn partitioning for a sphalerite + stannite-kesterite assemblage using the calibration of Nakamura and Shima (1982) and the occasional presence of minerals such as stephanite (T < 197 °C, Keighin and Honea 1969) in fahlore-bearing assemblages.

Declarations

Conflict of interest The authors declare that they have no known competing financial interests or personal relationships that could have appeared to influence the work reported in this paper.

References

Alves FEA, Neto AVC, Soares MB, Neuman R, da Silva GM, Varca AC, de Sampaio PAB, Silveira VD (2022) Genetic implications from textures, mineralogy, and geochemistry: the case of Zona Basal — a singular polymetallic occurrence in the Quadrilátero Ferrífero, Brazil: Contrib Min Pet 177:48. https://doi.org/10.1007/s00410-022-01913-w

Anikina EYu, Bortnikov NS, Klubnikin GK, Gamyanin GN, Prokof'ev VY (2016) The Mangazeya Ag–Pb–Zn vein deposit hosted in sedimentary rocks, Sakha-Yakutia, Russia: mineral assemblages, fluid inclusions, stable isotopes (C, O, S), and origin. Geol Ore Deposits 58(3):182–212. https://doi.org/10.1134/S1075701516030028

Aristov VV, Nekrasov AI (2010) Verkhoyansk silver-bearing province. Prospects of evolution and development of raw mineral base, in Mineral'nye resursy Rossii (Mineral Resources of Russia). Moscow Geoinform 1:21–29 (**(in Russian)**)

Arnold RG (1962) Equilibrium relations between pyrrhotite and pyrite from 325° to 743°C. Econ Geol 57:72–90. https://doi.org/10.2113/gsecongeo.57.1.72

Balabin AI, Sack RO (2000) Thermodynamics of (Zn, Fe)S sphalerite: a CVM approach with large basis clusters. Mineral Mag 64(5):923–943. https://doi.org/10.1180/002646100549751

Balabin AI, Urusov VS (1995) Recalibration of the sphalerite cosmobarometer: experimental and theoretical treatment. Geochim

Cosmochim Acta 59(7):1401–1410. https://doi.org/10.1016/0016-7037(95)00052-2

Balitskaya OV, Mozgova NN, Borodaev YuS, Efimov AV, Tsepin AI (1989) Dependence of the unit cell parameter of fahlores on the content of silver in them: Izvestiya Acad Sci USSR. Geological Series 9:112–120 (**in Russian**)

Barton PB Jr, Toulmin P (1966) Phase relations involving sphalerite in the Fe–Zn–S system. Econ Geol 61(5):815–849. https://doi.org/10.2113/gsecongeo.61.5.815

Beaudoin G, Sangster DF (1992) A descriptive model for silver-lead-zinc veins in clastic metasedimentary terranes. Econ Geol 87(4):1005–1021. https://doi.org/10.2113/gsecongeo.87.4.1005

Beaudoin G, Roddick JC, Sangster DF (1992) Eocene age for Ag–Pb–Zn–Au vein and replacement deposits of the Kokanee Range, southeastern British Columbia. Can J Earth Sci 29(1):3–14. https://doi.org/10.1139/e92-002

Belov NV, Pobedimskaya EA (1973) Essays in structural mineralogy: XXIV: Mineralogical collection, 27(1):3–9. (in Russian)

Biagioni C, George L, Cook N, Makovicky E, Moëlo Y, Pasero M, Sejkora J, Stanley CJ, Welch MD, Bosi F (2020) The Tetrahedrite Group: Nomenclature and Classification. Am Min 103(1):109–122. https://doi.org/10.2138/am-2020-7128

Boorman RS, Sutherland JK, Chernyshev LV (1971) New data on the sphalerite-pyrrhotite-pyrite solvus. Econ Geol 66:670–675. https://doi.org/10.2113/gsecongeo.66.4.670

Boyle RW (1965) Keno Hill-Galena Hill lead-zinc-silver deposits. Yukon Territory, Geol Survey Can, Bull, p 111

Butrymowicz DB, Manning JR, Read ME (1974) Diffusion in copper and copper alloys, Part II. Copper-silver and copper-gold systems. J Phys Chem Ref Data 3(2):527–602. https://doi.org/10.1063/1.3253145

Chinchilla D, Ortega L, Piña R, Merinero R, Moncada D, Bodnar RJ, Quesada C, Valverade A, Lunar R (2016) The Patricia Zn–Pb–Ag epithermal ore deposit: an uncommon type of mineralization in northeastern Chile. Ore Geol Rev 73(1):104–126. https://doi.org/10.1016/j.oregeorev.2015.10.026

Ebel DS, Sack RO (1994) Experimental determination of the free energies of formation of freibergite fahlores. Geochim Cosmochim Acta 58(4):1237–1242. https://doi.org/10.1016/0016-7037(94)90377-8

Ebel DS (1993, ms) Thermochemistry of fahlore (tetrahedrite) and biotite mineral solutions. West Lafayette, Indiana, Purdue University, Ph.D. thesis, 346 p.

Fan X, Case ED, Lu X, Morelli DT (2013) Room temperature mechanical properties of natural-mineral-based thermoelectric. J Material Sci 48(21):7540–7550. https://doi.org/10.1007/s10853-013-7569-1

Fleck RJ, Criss RE, Eaton GF, Cleland RW, Wavra CS, Bond WD (2002) Age and origin of base and precious metal veins of the Coeur d'Alene mining district, Idaho. Econ Geol 97:23–42. https://doi.org/10.2113/gsecongeo.97.1.23

Furdyna JF (1988) Dilute magnetic semiconductors. J Appl Phys 64(4):R29–R64. https://doi.org/10.1063/1.341700

Grove TL, Baker MB, Kinzler RJ (1984) Coupled CaAl-NaSi diffusion in plagioclase feldspar: experiments and applications to cooling rate speedometry. Geochim Cosmochim Acta 80(10):2113–2121. https://doi.org/10.1016/0016-7037(84)90391-0

Harlov DE, Sack RO (1995) Thermochemistry of Ag$_2$S–Cu$_2$S sulfide solutions: constraints derived from coexisting Sb$_2$S$_3$–bearing sulfosalts. Geochim Cosmochim Acta 59(21):4351–4365. https://doi.org/10.1016/0016-7037(95)00308-M

Indolev LN, Nevoisa GG (1974) Silver-lead deposits in Yakutia. Novosibirsk. Nauka, 250 p. (in Russian).

Jeanloz R, Johnson ML (1984) A note on the bonding, optical spectrum and composition of tetrahedrite. Phys Chem Min 11(1):52–54. https://doi.org/10.1007/BF00309375

Jian C-C, Zhang J, Ma X (2020) Cu-Ag alloy for engineering properties and applications based on the LSPR of metal nanoparticles. Royal Soc Chem Adv 10:13277–13285. https://doi.org/10.1039/D0RA01474E

Johnson M, Jeanloz R (1983) A brillouin zone model for compositional variation in tetrahedrite. Am Min 68:220–226

Johnson NE, Craig JR, Rimstidt JD (1988) Crystal Chemistry of Tetrahedrite. Am Min 73(3–4):389–397

Keighin CW, Honea RM (1969) The system Ag—Sb—S from 600° to 200°C. Min Deposita 4:153–171. https://doi.org/10.1007/BF00208050

Lusk J, Ford CE (1978) Experimental extension of the sphalerite geobarometer to 10 kbar. Am Min 78:516–519

Lynch JVG (1989a) Large-scale hydrothermal zoning reflected in the tetrahedrite-freibergite solid solution, Keno Hill Ag-Pb-Zn district, Yukon. Can Min 27:383–400

Lynch JVG (1989b, ms), Hydrothermal zoning in the Keno Hill Ag-Pb-Zn vein system: a study in structural geology, mineralogy and stable isotope geochemistry. Alberta, Canada, University of Alberta, Ph.D. thesis, 218 p. https://doi.org/10.7939/R38K75524

Lyubimtseva NG, Bortnikov NS, Borisovsky SE, Prokofiev VY, Vikent'eva OV (2018) Fahlore and sphalerite from the Darasun gold deposit in the Eastern Transbaikal Region, Russia: I. Mineral assemblages and intergrowths, chemical composition, and its evolution. Geol Ore Deposits 60(2):93–120. https://doi.org/10.1134/S1075701518020034

Lyubimtseva NG, Bortnikov NS, Borisovsky SE, Prokofiev (2020) Oscillatory Zoning in Tennantite-(Fe) at the Darasun Gold Deposit (Eastern Transbaikal Region, Russia). Geol Ore Deposits 62(3):177–203. https://doi.org/10.1134/S1075701520030046

Machatschki F (1928) Formel und Kristallstruktur des tetraedrites. Norsk Geol Tidsskrift 10:23

Makovicky E (2006) Crystal structures of sulfides and other Chalcogenides, In DJ Vaughan, (ed), sulfide mineralogy and geochemistry. Rev Min Geochem 61:7–126. https://doi.org/10.1515/9781501509490-003

Makovicky E, Skinner BJ (1978) Studies of the sulfosalts of copper VI. Low-temperature exsolution in synthetic tetrahedrite solid solution, Cu12+ xSb4+ yS13. Can Min 16(4):611–623

Moëlo Y, Makovicky E, Mozgova NN, Jambor JL, Cook N, Pring A, Paar WH, Nickel EH, Gräser S, Karup-Moller S, Balic-Zunic T, Mumme WG, Vurro F, Topa D, Bindi L, Bente K, Shimizu M (2008) Sulfosalt systematics: a review. Report of the sulfosalt subcommittee of the IMA Commission on Ore Mineralogy. Eur J Min 20(1):7–46. https://doi.org/10.1127/0935-1221/2008/0020-1778

Nakamura F, Shima H (1982, abstract) Fe and Zn partitioning between sphalerite and stannite: Joint meeting of the Society of Mining Geology of Japan, Association of Mineralogy, Petrology and Economic Geology, and Mineralogical Society of Japan, A-8 (in Japanese)

Nekrasov AI (2017) Geological-genetic models of polychronous and polygenic gold and silver deposits of the Verkhoyansk-Kolyma folded region (example of Mangazeyskoye silver ore field). Otechestvennaya Geologiya 1:39–53 (**in Russian**)

O'Leary MJ, Sack RO (1987) Fe-Zn exchange reaction between tetrahedrite and sphalerite in natural environments. Contrib Min Pet 96(4):415–425. https://doi.org/10.1007/BF01166687

Osadchii EG, Gorbaty JM (2010) Raman spectra and unit cell parameters of sphalerite solid solutions (Fe$_x$Zn$_{1-x}$S). Geochim Cosmochim Acta 74(2):568–573. https://doi.org/10.1016/j.gca.2009.10.022

Pankratz LB, King EG (1965) High-temperature heat contents and entropies of two zinc sulfides and four solid solutions of zinc and iron sulfides. Bureau Mines Rept Invest 6708:1–8

Pattrick RAD, Hall AJ (1983) Silver substitution into synthetic zinc, cadmium and and iron tertahedrites. Min Mag 47:441–451

Pauling L, Neuman EW (1934) The crystal structure of binnite, (Cu, Fe)$_{12}$As$_4$S$_{13}$, and the chemical composition and structure of minerals of the tetrahedrite group. Zeit Kristallogr-Crystal Mater 88(1):54–62. https://doi.org/10.1524/zkri.1934.88.1.54

Pring A, Tarantino SC, Tenailleau C, Etschmann B, Carpenter MA, Zhang M, Liu Y, Withers RL (2008) The crystal chemistry of Fe-bearing sphalerites: an infrared spectroscopic study. Am Min 93(4):591–597. https://doi.org/10.2138/am.2008.2610

Qu K, Sima X, Gu X, Sun W, Fan G, Hou Z, Ni P, Wang D, Yang Z, Wang Y (2021) Kenoargentotetrahedrite-(Zn), IMA 2020–075. CNMNC Newsletter 59. Min Mag. https://doi.org/10.1180/mgm.2021.5

Riley JF (1974) The tetrahedrite-freibergite series with reference to the Mount Isa Pb-Zn-Ag orebody. Min Deposita 9(2):117–124. https://doi.org/10.1007/BF00207969

Rozhdestvenskaya IV, Zayakina NV, Samusikov VP (1993) Crystal structure features of minerals from a series of tetrahedrite-freibergite. Mineralgiceskij Zhurnal 15:9–17 (**in Russian**)

Ruan B, Lv X, Yang W, Liu S, Yu Y, Wu C, Adam MMA (2015) Geology, geochemistry and fluid inclusions of the Bianjiadayuan Pb-Zn-Ag deposit, Inner Mongolia, NE China: implications for tectonic setting and metallogeny. Ore Geol Rev 71:121–137

Sack RO (1992) Thermochemistry of tetrahedrite-tennantite fahlores. In: Ross NL, Price GD (eds) The Stability of Minerals. Chapman and Hall, London, pp 243–266

Sack RO (2000) Internally consistent database for sulfides and sulfosalts in the system Ag$_2$S-Cu$_2$S-ZnS-Sb$_2$S$_3$-As$_2$S$_3$. Geochim Cosmochim Acta 64(22):3803–3812. https://doi.org/10.1016/S0016-7037(00)00468-3

Sack RO (2002) Note on "Large-scale hydrothermal zoning reflected in the tetrahedrite-freibergite solid solution, Keno Hill Ag-Pb-Zn District, Yukon" by J.V. Gregory Lynch Can Min 40:1717–1719. https://doi.org/10.2113/gscanmin.40.6.1717

Sack RO (2005) Internally consistent database for sulfides and sulfosalts in the system Ag$_2$S– Cu$_2$S–ZnS–FeS–Sb$_2$S$_3$–As$_2$S$_3$: Update. Geochim Cosmochim Acta 69:1157–1164. https://doi.org/10.1016/j.gca.2004.08.017

Sack RO (2017) Fahlore thermochemistry: gaps inside the (Cu, Ag)10(Fe, Zn)2(Sb, As)4S13 cube. Petrol 25(5):498–515. https://doi.org/10.1134/S0869591117050071

Sack RO (2021) Thermochemistry of melilites I. Towards resolving an inconsistency in nebular condensation calculations. Am J Sci 321(4):424–457. https://doi.org/10.2475/04.2021.02

Sack RO, Ebel DS (1993) As-Sb exchange energies in tetrahedrite-tennantite fahlores and bournonite-seligmannite solid solutions. Min Mag 57:635–642. https://doi.org/10.1180/minmag.1993.057.389.07

Sack RO, Ebel DS (2006) Thermochemistry of Sulfide Mineral Solutions, In: DJ Vaughan (ed), Sulfide Mineralogy and Geochemistry. Rev Min and Geochem 61:265–364. https://doi.org/10.1515/9781501509490-007

Sack RO, Ghiorso MS (2017) Ti^{3+} - and Ti^{4+} -rich fassaites at the birth of the solar system: thermodynamics and applications. Am J Sci 317(7):807–845. https://doi.org/10.2475/07.2017.02

Sack RO, Goodell PC (2002) Retrograde reactions involving galena and Ag−sulfosalts in a zoned ore deposit, Julcani, Peru. Min Mag 66:1043–1062. https://doi.org/10.1180/0026461026660076

Sack RO, Lichtner PC (2009) Constraining compositions of hydrothermal fluids in equilibrium with polymetallic ore forming sulfide assemblages. Econ Geol 104(8):1249–1264. https://doi.org/10.2113/gsecongeo.104.8.1249

Sack RO, Lichtner PC (2010) Constraining compositions of hydrothermal fluids in equilibrium with polymetallic ore forming sulfide assemblages: Erratum. Econ Geol 104(8):1249–1264. https://doi.org/10.2113/gsecongeo.105.1.249

Sack RO, Loucks RR (1985) Thermodynamic properties of tetrahedrite-tennantites: constraints on the interdependence of the Ag-Cu, Fe-Zn, Cu-Fe, and As-Sb exchange reactions. Am Min 70:1270–1289

Sack RO, Kuehner SM, Hardy LS (2002) Retrograde Ag-enrichment in fahlores from the Coeur d'Alene mining district, Idaho, USA. Min Mag 66:215–229. https://doi.org/10.1180/0026461026610024

Sack RO, Lynch JGV, Foit FF Jr (2003) Fahlore as a petrogenetic indicator: Keno Hill Ag-Pb-Zn district, Yukon, Canada. Min Mag 67:1023–1038. https://doi.org/10.1180/0026461036750141

Sack RO, Fredericks R, Hardy LS, Ebel DS (2005) Origin of high-silver fahlores from the Galena Mine Wallace, Idaho, USA. Am Min 90(5–6):1000–1007. https://doi.org/10.2138/am.2005.1651

Schenck R, von der Forst P (1939) Gleichewichtsstudien an erzbinende sulfide. II Z Anorg Allg Chem 241(2–3):145–157. https://doi.org/10.1002/zaac.19392410201

Schenck R, Hoffmann I, Knepper W, Vogler H (1939) Gleichewichtsstudien uber erzbinende sulfide. I Z Anorg Allg Chem 240(2):178–197. https://doi.org/10.1002/zaac.19392400211

Scott SD (1973) Experimental calibration of the sphalerite geobarometer. Econ Geol 68(4):466–474. https://doi.org/10.2113/gsecongeo.68.4.466

Scott SD, Barnes HL (1971) Sphalerite geothermometry and geobarometry. Econ Geol 66(4):653–569. https://doi.org/10.2113/gsecongeo.66.4.653

Sejkora J, Biagioni C, Vrtiška L, Moëlo Y (2021a) Zvěstovite -(Zn), Ag$_6$(Ag$_4$Zn$_2$)As$_4$S$_{13}$, a new tetrahedrite-group mineral from Zvěstov. Czech Republic Min Mag 85(5):716–724. https://doi.org/10.1180/mgm.2021.57

Sejkora J, Biagioni C, Števko M, Raber T, Roth P (2021b) Argento-tetrahedrite-(Zn), IMA 2020–069. CNMNC Newsletter 59. Min Mag. https://doi.org/10.1180/mgm.2021b.5

Sejkora J, Biagioni C, Števko M, Raber T, Roth P, Vrtiška (2022) Argentotetrahedrite-(Zn), Ag$_6$(Cu$_4$Zn$_2$)Sb$_4$S$_{13}$, a new member of the tetrahedrite group. Min Mag 86:319–330. https://doi.org/10.1180/mgm.2022.21

Shimada N, Hirowatari F (1972) Argentian tetrahedrite from the Taishu-Shigekuma mine, Tsushima Island, Japan. Min J 7(1):77–97

Shimizu M, Shikazono F (1985) Iron and Zinc Partitioning between Coexisting Stannite and Sphalerite: a Possible Indicator of Temperature and Sulfur Fugacity. Min Deposita 20(4):314–320. https://doi.org/10.1007/BF00204292

Smirnov SS (1962) Ore deposits and metallogeny of the Eastern regions of the USSR, Moscow. The USSR Acad Sci, 359 p. (in Russian)

Swinkels L, Schulz-Isenbeck J, Frenzel M, Gutzmer J, Burisch M (2021) Spatial and temporal evolution of the freiberg epithermal Ag-Pb-Zn District, Germany. Econ Geol 116(7):1649–1667

Tatsuka K, Morimoto N (1977) Tetrahedrite stability relations in the Cu-Fe-Sb-S system. Am Min 62(11–12):1101–1109

Toulmin P III, Barton PB Jr, Wiggins LB (1991) Commentary on the sphalerite geothermometer. Am Min 76:1038–1051

Twardowski A (1990) Magnetic properties of Fe-based diluted semiconductors. J Appl Phys 67:5108–5113. https://doi.org/10.1063/1.344685

Twardowski A, Lewicki A, Arciszewska M, de Jonge WJM, Swagten HJM, Demianiuk M (1988) Magnetic susceptibility of iron-based semimagnetic semiconductors. Phys Rev B 38:10749. https://doi.org/10.1103/PhysRevB.38.10749

Verduch AG, Wagner C (1957) Contributions to the thermodynamics of the systems PbS–Sb$_2$S$_3$, Cu$_2$S–Sb$_2$S$_3$, Ag$_2$S–Sb$_2$S$_3$, and Ag–Sb. J Phys Chem 61(5):558–562. https://doi.org/10.1021/j150551a011

Wang X (2014, ms) The study of the Metallogenic characteristics and genesis of the Bianjiadayuan Ag-Pb-Zn deposit in Inner Mongolia,

China. Beijing, China, China University of Geosciences, M.S. thesis, 85 p. (in Chinese with English)

Welch MD, Stanley CJ, Spratt J, Mills SJ (2018) Rozhdestvenskayaite $Ag_{10}Zn_2Sb_4S_{13}$ and argentotetrahedrite $Ag_6Cu_4(Fe^{2+}, Zn)_2Sb_4S_13$: two Ag-dominant members of the tetrahedrite group. Eur J Min 30(6):1163–1172. https://doi.org/10.1127/ejm/2018/0030-2773

White BG (1998) New tricks for an old elephant: Revising concepts of Coeur d'Alene geology. Mining Eng 50(8):27–35

Wright K, Gale JD (2010) A first principles study of the distribution of iron in sphalerite. Geochim Cosmochim Acta 74(12):3514–3520. https://doi.org/10.1016/j.gca.2010.03.014

Wu P, Gu X, Qu K, Yang H, Wang Y (2021) Argentotetrahedrite-(Hg), IMA 2020–079. CNMNC Newsletter 59. Min Mag. https://doi.org/10.1180/mgm.2021.5

Wuensch BJ (1964) The crystal structure of tetrahedrite, $Cu_{12}Sb_4S_{13}$. Z Kristallogr-Crystal Mater 119(5–6):437–453. https://doi.org/10.1524/zkri.1964.119.5-6.437

Wuensch BJ, Takeuchi Y, Nowacki W (1966) Refinement of the crystal structure of binnite, $Cu_{12}As_4S_{13}$. Z Kristallogr-Crystal Mater 123(1):1–20. https://doi.org/10.1524/zkri.1966.123.16.1

Zhai D (2022) Fluid-rock interactions leading to the formation of the epithermal Ag-Pb-Zn veins: a perspective of thermodynamic modeling. Fundam Res. https://doi.org/10.1016/j.fmre.2022.03.004

Zhai D, Jiajin L, Cook NJ, Wang X, Yang Y, Zhang A, Jiao Y (2019) Mineralogical, textural, sulfur and lead isotope constraints on the origin of Ag-Pb-Zn mineralization at Bianjiadayuan, Inner Mongolia, NE China. Min Deposita 54:47–66. https://doi.org/10.0007/s00126-018-0804-6